MATERIALS CHEMISTRY
FRONTIERS

REVIEW

View Article Online
View Journal | View Issue

Cite this: *Mater. Chem. Front.*, 2023, **7**, 5247

Porous organic cages for gas separations

Wenjing Wang, [ac] Kongzhao Su *[ac] and Daqiang Yuan *[abc]

Received 28th June 2023,
Accepted 25th July 2023

DOI: 10.1039/d3qm00715d

rsc.li/frontiers-materials

Gases have played a crucial role in various industries, spanning from manufacturing and medicine to electronics. In these industries, the attainment of pure gases through effective separation methods has been recognized as essential. Porous materials-based adsorption and separation technologies have garnered significant attention due to their advantageous features, including low energy consumption and simplified operational procedures. Among these materials, porous organic cages (POCs) have emerged as a promising class, constructed by individually designed macromolecules possessing inherent cavities that are tailor-made, soluble, easily regenerated, and amenable to precise modifications. Analogous to well-established porous framework materials like zeolites, metal–organic frameworks (MOFs), and covalent organic frameworks (COFs), POCs have exhibited their intrinsic potential for gas separation applications in recent years. In this review, we delve into the progress achieved in the realm of POCs, with a particular focus on their utilization for selective gas separation. Moreover, we present an outlook on the future prospects of this field, along with the existing challenges that demand further attention.

1. Introduction

Separation technology is of paramount importance in contemporary society for various industries to extract pure substances from chemical mixtures. Examples of such applications include the separation of hydrocarbons from crude oil, alkenes from alkanes, greenhouse gases from dilute emissions, as well as the extraction of various derivatives and metals from different sources.[1] Gases, in particular, play a fundamental role in the production of chemicals, including fuels, plastics, and polymers, as well as in the domains of petrochemicals, pharmaceuticals, and nuclear industries, where they serve as neutron moderators.[2] Traditional methods for gas separation rely on cryogenic distillation, which involves repetitive cycles of evaporation and condensation,[3,4] resulting in high energy consumption, environmental concerns, and potential generation of secondary by-products. Consequently, alternative gas purification methods that are both cost- and energy-efficient are urgently needed.

[a] *State Key Laboratory of Structural Chemistry, Fujian Institute of Research on the Structure of Matter, Chinese Academy of Sciences, Fuzhou, 350002, China. E-mail: skz@fjirsm.ac.cn, ydq@fjirsm.ac.cn*
[b] *Fujian Science and Technology Innovation Laboratory for Optoelectronic Information of China, Fuzhou 350108, Fujian, P. R. China*
[c] *University of the Chinese Academy of Sciences, Beijing, 100049, China*

Wenjing Wang

Wenjing Wang received his PhD degree in 2017 from Fujian Institute of Research on the Structure of Matter (FJIRSM), Chinese Academy of Sciences (CAS), under the supervision of Prof. Daqiang Yuan. He is now an associate professor at the FJIRSM. Currently, his research interests focus on the design and synthesis of crystalline porous materials for gas separation and fluorescence sensor applications.

Kongzhao Su

Kongzhao Su received his PhD degree in 2015 from Fujian Institute of Research on the Structure of Matter (FJIRSM), Chinese Academy of Sciences (CAS), under the supervision of Prof. Maochun Hong. He is now a Professor at FJIRSM, and also a member of the Youth Innovation Promotion Association CAS. His current research interests include the rational design of robust porous organic cages (POCs), and their applications in energy and environmental areas.

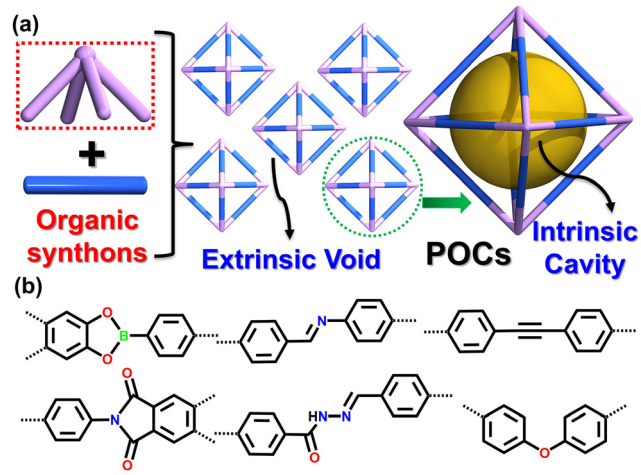

Fig. 1 (a) Synthesis and characteristics of POCs. (b) Common covalent linkages in construction of POCs.

In recent years, porous materials have emerged as a promising solution to address gas storage and separation challenges. Notable porous adsorbents encompass a range of materials, including metal-containing framework adsorbents like zeolites and metal–organic frameworks (MOFs),[5–10] porous organic adsorbents such as porous organic polymers (POPs),[11–13] covalent-organic frameworks (COFs),[14–16] and hydrogen-bonded organic frameworks (HOFs),[17–19] and molecular cage adsorbents like porous organic cages (POCs)[20] and metal–organic cages (MOCs).[21] MOFs have witnessed the most rapid development in the field of gas separation due to their remarkable porosity, tunable pore structures, and unsaturated metal sites, leading to their successful applications in various separations such as carbon dioxide (CO_2) separation,[22,23] alkene purification,[24] noble gas separation,[25] and isotope separation.[26] However, despite their accomplishments, MOFs face challenges concerning cost, regeneration, stability, and selectivity, making it crucial to explore alternative porous materials for gas separation. It is worth noting that the progress in the development of other porous materials has been notably slower compared to MOFs, despite their inherent advantages. For instance, zeolites offer cost-effectiveness and easy availability, while porous organic materials possess a metal-free nature and native nonpolar/inert pore surfaces. POPs exhibit high stability, and HOFs and POCs allow for easy regeneration and tunability in fine-level pore sizes, respectively. Therefore, it is essential to investigate the gas purification capabilities of these materials to foster the advancement of diverse classes of porous materials in the field of gas separation.

Among the porous materials, POCs are constructed through covalent linkages of organic synthons to form discrete macromolecules with intrinsically hollow cavities (Fig. 1).[27–34] This distinctive structure provides POCs with several advantages that include solution processing, regeneration, and post-synthesis modification,[35–42] compared to other porous framework materials. Organic cage compounds were first reported by the Nobel Prize-winning chemist Jean-Marie Lehn in 1969, who presented the first example of organic cage molecules constructed from crown ether for cation binding.[43] However, it was not until 2009 that Cooper's group confirmed the ability of isolated shape-persistent organic cages to serve as porous solids for gas storage.[44] Since then, there has been a rapid increase in the number of POCs with different topologies, shapes, and surface areas, attracting significant attention over the past decade.[45–73] The common methods used to synthesize POCs can be categorized into two types: irreversible bond formation and reversible bond formation, which mainly include several condensation reactions.[20] Both methods have been extensively reviewed in recent publications.

POCs, as a relatively new sub-class of porous materials, share many advantages with other porous materials including low density, high surface area and pore volume, tunable window and cavity sizes, and the ability for easy and precise modification. Additionally, POCs show promising potential for numerous applications such as molecular recognition, membranes, catalysis, and separation.[74–85] Despite prior reviews covering several applications, there remains an insufficient amount of coverage regarding the efficient gas-selective separation achieved by POCs. Similar to zeolites, MOFs, and COFs, POCs also exhibit gas storage and separation capabilities, fundamental attributes of porous materials. However, POCs are distinct in their construction as discrete molecules held together by weak intermolecular interactions, which results in their porosity arising not only from intrinsic cavities but from extrinsic voids or channels that result from inefficient molecule packing in the solid state. This feature makes POCs vulnerable to structural changes that may significantly impact their porosity and performance in gas storage and separation. Over the last decade, the Brunauer–Emmett–Teller (BET) surface area of POCs has increased from 624 $m^2\ g^{-1}$ to 3758 $m^2\ g^{-1}$, displaying the ability to selectively store and separate gases such as CO_2, hydrocarbons, noble gases, and isotope gases as shown on Fig. 2. Zhang *et al.* recorded the first shape-persistent prismatic molecular cage capable of high selectivity for CO_2 over N_2 adsorption in 2010.[86] Since then, Mastalerz *et al.* has developed several shape-persistent POCs that exhibit selective CO_2 separation capabilities,[87] whereas Cooper *et al.* reported, in 2014, that an imine-linked tetrahedral POC (**CC3**) was effective in effectively separating noble gas

Daqiang Yuan

Daqiang Yuan obtained his PhD degree from Fujian Institute of Research on the Structure of Matter, Chinese Academy of Sciences, under the supervision of Prof. Maochun Hong in 2006. After finishing a postdoctoral fellowship at Miami University and Texas A&M University with Prof. Hong-Cai Joe Zhou, he joined Fujian Institute of Research on the Structure of Matter as a full professor in 2011. His main research interest is the designed synthesis and applications of new porous materials, including metal–organic cages, porous organic cages, and metal–organic frameworks.

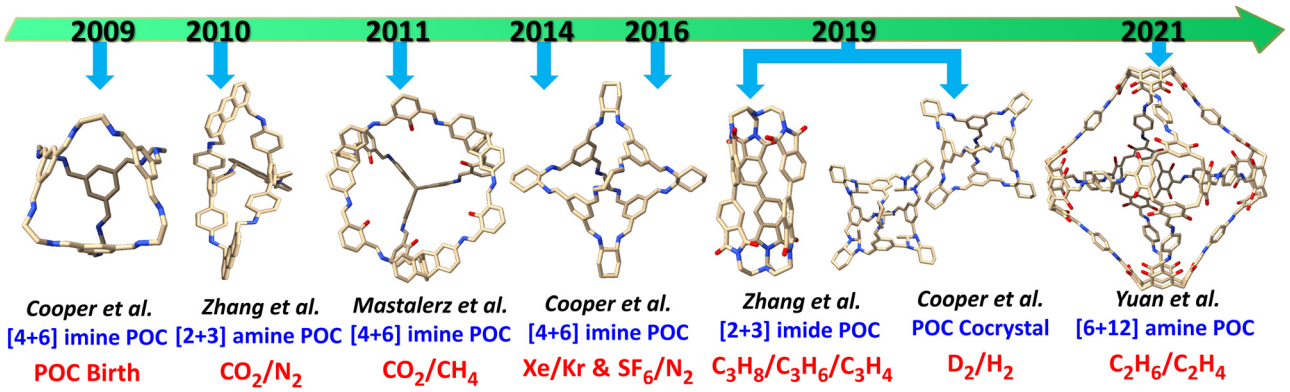

Fig. 2 Timeline of POCs for gas separation applications. Carbon is orange, oxygen red, nitrogen blue, and fluorine green. Hydrogen atoms and alkyl groups are omitted for clarity.

Xenon (Xe) and Krypton (Kr).[88] Moreover, they showed successful separation of greenhouse gas sulfur hexafluoride (SF_6) and N_2 in 2016,[89] and gaseous isotope mixtures (D_2/H_2) in 2019 by fine-tuning the internal cavities of POCs.[90] Furthermore, Zhang *et al.* achieved efficient separation of binary or ternary C3 hydrocarbon mixtures using a soft imide-based POC (**NKPOC-1**) with gate-opening behavior in 2019.[91] Yuan *et al.* developed a robust ethane-trapping POC (**CPOC-301**) in 2021, enabling one-step purification of high-purity ethylene (C_2H_4) from ethane (C_2H_6) and C_2H_4 mixture.[92] They also discovered the solvatomorphism, which influenced acetylene (C_2H_2) and CO_2 separation in **CPOC-101**.[93] In 2022, Mastalerz *et al.* fine-tuned the fluorinated side-chains on the windows of imine-linked POCs,[94] subsequently improving the separation of fluorinated alkanes. This review aims to provide a comprehensive overview of the significant progress made by POCs in gas separation. It is divided into distinct sections covering CO_2 separation, hydrocarbon purification, rare gas separation, fluorinated greenhouse gas separation, and D_2/H_2 isotope separation. Additionally, we address remaining challenges and offer an outlook to stimulate further development of POCs in gas separation.

2. POCs for gas separations

Gas molecule separation is a challenging technological feat, particularly when the molecules possess similar sizes and shapes. However, highly porous materials utilized for adsorptive separation have become an alternative technology due to the lower energy consumption. POCs, with their exceptional characteristics, offer promising potential for highly efficient gas separation. In this section, we aim to provide an overview of the significant advancements made in POCs regarding the separation of various gases, such as CO_2, light hydrocarbons, Xe/Kr, fluorinated greenhouse gases and D_2/H_2.

2.1. CO_2 separation

The accelerated increase in atmospheric CO_2 concentration caused by climate change has recently received substantial attention. In response, porous materials that use physical adsorption are being considered as promising solutions for CO_2 capture. POCs, as a new type of porous material, have also been successfully used in separating CO_2/N_2.[95–98]

In 2010, Zhang *et al.* published a study which reported the use of prismatic molecule **cage 6** as an effective medium for CO_2 and N_2 separation.[86] They observed that CO_2 uptake capacity was 4.46 $cm^3\ g^{-1}$, while N_2 exhibited negligible adsorption at 0.061 cm^3. The CO_2/N_2 adsorption selectivity was calculated to be 73, highlighting a profound affinity for CO_2 over N_2 during adsorption. Later, they successfully produced a series of new organic cage compounds (**1–4**) using a one-pot reversible imine condensation reaction between triamines and dialdehydes,[99] followed by hydride reduction of the resulting imine to amine bonds. The triamine moieties functioned as the top and bottom panels of a trigonal prism, while the dialdehyde moieties served as the three lateral edges. The N_2 adsorption isotherms at 77 K revealed that these materials had no pores for N_2 gas, as indicated by a BET surface area of less than 10 $m^2\ g^{-1}$. **Cage 4** had the lowest N_2 uptake while also displaying a comparable adsorption capacity for CO_2, resulting in the highest CO_2/N_2 adsorption selectivity with a ratio of 138/1. The selectivity in gas adsorption observed could be attributed to the density of amino groups within the cage molecule and the size of the cage cavity. The amino group density predominantly governed the uptake of CO_2, whereas the capacity for N_2 adsorption related to the dimensions of the molecular prisms.

Cooper *et al.* reported a new propeller-shaped organic cage known as **CC6** in 2011,[100] produced *via* a one-step [2+3] cycloimination reaction between 1,3,5-tri(4-formylphenyl)benzene and 1,5-pentanediamine. The resulting **CC6** had a moderate apparent BET surface area of 99 $m^2\ g^{-1}$. Examination of the N_2 adsorption isotherm at 300 K and 1.2 bar revealed a low gas uptake of 0.08 mmol g^{-1}. Conversely, the CO_2 adsorption capacity of **CC6** under the same conditions was determined to be 0.90 mmol g^{-1}. Using these isotherms, the ideal selectivity for CO_2/N_2 at 300 K and 1 bar was calculated to be 11.

In addition to reversible imine condensation, Zhang *et al.* successfully produced a tricyclooxacalixarene cage, named **cage 1**, in 2015 *via* a one-pot S_NAr reaction involving tetrahydroxytetraphenylethylene and 2,6-dichloropyridine-3,5-dicarbonitrile

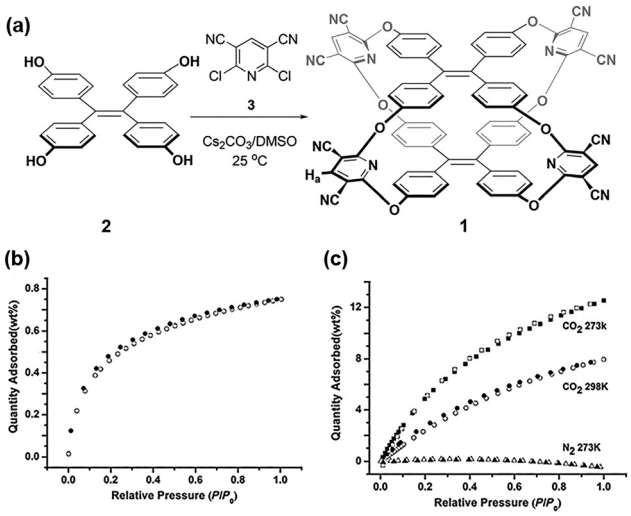

Fig. 3 (a) Synthesis of TPE-based tricyclooxacalixarene **cage 1**. (b) H_2 sorption isotherms at 77 K. (c) CO_2 and N_2 sorption isotherms at 273 K and 298 K. Reproduced with permission from ref. 101. Copyright 2015, Wiley.

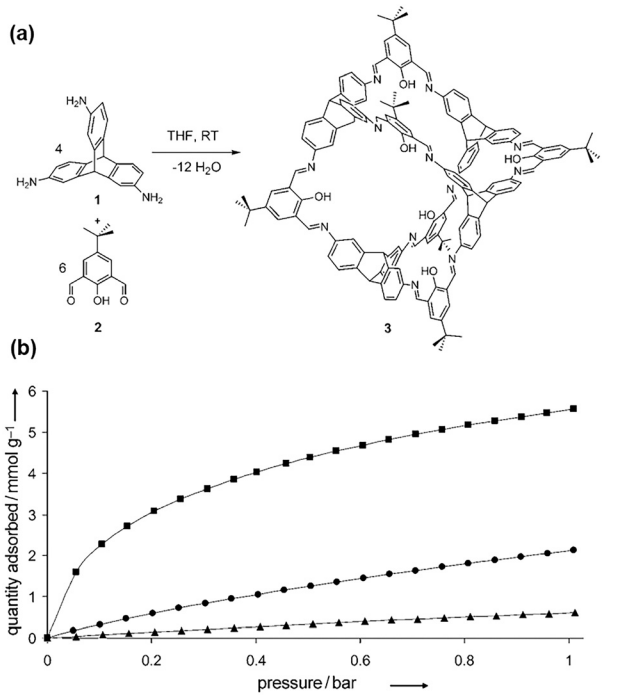

Fig. 4 (a) Synthesis of **cage 3**. (b) Gas adsorption isotherms of H_2 (square, 77 K), CO_2 (circle, 273 K), and CH_4 (triangle, 273 K) for cage compound **3**. Reproduced with permission from ref. 87. Copyright 2011, Wiley.

(Fig. 3).[101] This tricyclic cage had a grid-like porous architecture and demonstrated remarkable adsorption capacity for CO_2, accompanied by high selectivity towards CO_2/N_2. Despite having a moderate surface area (432 $m^2\ g^{-1}$), **cage 1** could adsorb 84 $cm^3\ g^{-1}$ (0.75 wt%) of H_2 and 62.7 $cm^3\ g^{-1}$ (12.5 wt%) of CO_2 at 1.0 bar. The superior CO_2 adsorption performance of **cage 1** can be attributed to the optimal congruence between its microporous structure and the dimensions of CO_2, as well as the electron-rich nature of nitrogen and oxygen atoms within the cage framework, which facilitate local-dipole/quadrupole interactions with CO_2. The analysis of the initial slopes of the adsorption isotherms yielded a calculated CO_2/N_2 selectivity of 80 for **cage 1**.

In 2018, a new cage (**cage 5**) was synthesized through a reaction between di(*p*-methylphenyl)-di(*p*-aminophenyl)ethylene and 2,6-pyridinediformyl chloride.[102] **Cage 5** has a BET surface area of 347 $m^2\ g^{-1}$ and displays considerable CO_2 uptake of 39.7 $cm^3\ g^{-1}$ at 273 K and 1 bar, equating to approximately six CO_2 molecules per cage, with each CO_2 molecule binding to one pyridyl ring. Moreover, the N_2 adsorption under the same conditions was negligible, resulting in an excellent CO_2/N_2 selectivity of up to 32.

In 2020, Zhang *et al.* synthesized a triptycene-based cage (**TC**) using copper-mediated modified Eglinton-Glaser oxidative coupling reaction.[103] The initial structure of **TC** exhibited limited N_2 adsorption at 77 K and a relatively low BET surface area of only 7 $m^2\ g^{-1}$. However, by rapidly precipitating **TC-rp** from a methanol/dichloromethane solution, it transformed into a porous state, increasing the BET surface area to 653 $m^2\ g^{-1}$. **TC-rp** also displayed noteworthy CO_2 uptake capacities, with values of 42.3 $cm^3\ g^{-1}$ at 273 K and 33.6 $cm^3\ g^{-1}$ at 298 K. Based on these measurements, the CO_2/N_2 selectivity of **TC-rp** was found to be 4.8 at 273 K.

Although it is primarily composed of methane (CH_4), natural gas often contains significant amounts of CO_2 that must be extracted to increase its heating value and prevent pipeline corrosion. POCs have also been utilized in the separation of CO_2/CH_4.[104,105] In 2011, Mastalerz *et al.* examined the separation characteristics of CO_2/CH_4 using **cage 3**, which they synthesized through a one-pot Schiff base condensation reaction involving triamine and salicylbisaldehyde (Fig. 4).[87] **Cage 3** had a calculated BET surface area of 1375 $m^2\ g^{-1}$ and a Langmuir surface area of 1566 $m^2\ g^{-1}$. At 77 K and 1 bar, the H_2 adsorption capacity was 5.60 mmol g^{-1}. At the same conditions (273 K and 1 bar), the adsorption capacity of CO_2 was 2.10 mmol g^{-1}, while only 0.61 mmol g^{-1} of CH_4 was adsorbed. The marked difference in adsorption capacity between CO_2 and CH_4 implies the usefulness of **cage 3** in removing CO_2 from natural gas and enhancing CH_4 content. The authors credit the hydroxy groups inside the cages for the high CO_2/CH_4 selectivity (10 : 1 w/w) of **cage 3**. Subsequently, a new exo-functionalized [4+6] **cage 5** was reported, with a specific surface area of 919 $m^2\ g^{-1}$, which exhibited high selectivity for CO_2/CH_4. At 273 K and 1 bar, **cage 5** adsorbs 3.37 mmol g^{-1} CO_2 and only 0.66 mmol g^{-1} CH_4.[96]

Yuan *et al.* recently introduced two POCs called **CPOC-105** and **CPOC-106** constructed using two C4RACHO atoms with four *p*-xylylenediamine and *m*-xylylenediamine linkers,[106] respectively. The corresponding BET surface areas, calculated using CO_2 sorption at 196 K, were 277 and 218 $m^2\ g^{-1}$ for **CPOC-105** and **CPOC-106**, respectively. At 298 K and 1 bar, **CPOC-105** and **CPOC-106** showed higher adsorption capacities for CO_2 than CH_4, with 44 $cm^3\ g^{-1}$ *vs.* 17 $cm^3\ g^{-1}$ for **CPOC-105** and 37 $cm^3\ g^{-1}$ *vs.* 20 $cm^3\ g^{-1}$ for **CPOC-106**. Using Ideal Adsorbed Solution Theory (IAST) results under 1 bar, the CO_2/CH_4 selectivity values were

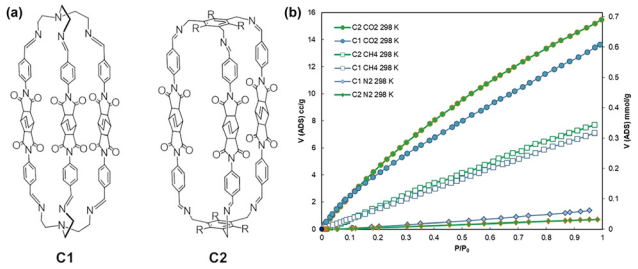

Fig. 5 (a) Sketches of **C1** and **C2** (R = ethyl). (b) Overlay of CO_2, CH_4, and N_2 adsorption isotherms, measured at 298 K. Reproduced with permission from ref. 107. Copyright 2022, Wiley.

calculated to be 4.5 for **CPOC-105** and 3.1 for **CPOC-106.** Dynamic breakthrough experiments were used to validate the superior separation performance of **CPOC-105.**

Amendola *et al.* presented two novel imide/imine organic cages, named **C1** and **C2** (Fig. 5),[107] synthesized through a [2+3] imine condensation reaction using two distinct polyamines and a novel dialdehyde compound incorporating a rigid bicyclo[2.2.2] oct-7-ene-2,3,5,6-tetracarboxydiimide core. At 298 K, the CO_2 adsorption capacities of **C1** and **C2** were 0.61 mmol g^{-1} and 0.69 mmol g^{-1}, respectively, while the adsorption capacities of CH_4 and N_2 were much lower. **C1** and **C2** demonstrated positive results in terms of CO_2/N_2 selectivity, with IAST selectivity values of 41 and 32, respectively, for CO_2/N_2 (15 : 85) mixtures. Moreover, both cages showed potential as fillers for mixed-matrix membranes (MMMs) in combination with polymers such as PEEK-WC and Matrimid® 9725. By incorporating **C1** and **C2** into Matrimid® 9725, CO_2/CH_4 selectivity was improved, and inclusion in PEEK-WC enhanced CO_2/N_2 selectivity.

In 2021, Mastalerz *et al.* conducted an investigation on chiral self-sorting of large cubic [8+12] salicylimine cages (Fig. 6).[108] The cages formed *via* the condensation of eight chiral C_3-symmetric TBTQ-tris(salicylaldehydes) with 12 *p*-phenylenediamine. Notably, only three isomers were observed: **(P)-4**, **(M)-4**, and **(P,M)-4**. The comparison between the two enantiomeric cages, **(P)-4** and **(M)-4**, revealed that they had similar BET surface area of 1212 and 1126 m^2 g^{-1}, respectively. At 273 K and 1 bar, **(P)-4** had an adsorption capacity of 61.1 cm^3 g^{-1} for CO_2 and 18.2 cm^3 g^{-1} for CH_4, while **(M)-4** had an adsorption capacity of 63.6 cm^3 g^{-1} for CO_2 and 19.7 cm^3 g^{-1} for CH_4. **(P)-4** had a CO_2/CH_4 selectivity of 7.6 and a CO_2/N_2 selectivity of 24.9, while **(M)-4** had a CO_2/CH_4 selectivity of 7.4 and a CO_2/N_2 selectivity of 24.7. A comparison between **(P,M)-4_1** and **(P,M)-4_2** yields intriguing insights. While **(P,M)-4_2** has higher crystallinity and a greater specific surface area, it shows lower selectivity. Specifically, it has selectivity values of 5 for CO_2/CH_4 and 12.3 for CO_2/N_2, compared to **(P,M)-4_1**, which has selectivity values of 7.1 for CO_2/CH_4 and 28.0 for CO_2/N_2. This finding emphasizes that a higher degree of crystallinity doesn't always mean superior material properties compared to an amorphous counterpart.

The structural stability of POCs is crucial in determining their gas separation performance. A highly acid and base-stable shape-persistent porous carbamate **cage 3** was introduced in 2017.[109] In addition, **cage 3** is capable of stability even in hot 1 M hydrochloric acid and in concentrated hydrochloric acid at room temperature without decomposition. Despite its low specific surface area, **cage 3** exhibited good selectivity towards CO_2/CH_4, adsorbing 58 cm^3 g^{-1} CO_2 and 21.8 cm^3 g^{-1} CH_4 at 273 K and 1 bar. In 2019, Mastalerz *et al.* synthesized a large shape-persistent [4+6] amide **cage 4**. The cages' chemical robustness enabled post-functionalization under harsh conditions, resulting in the formation of demethylated **cage 7**, brominated **cage 8**, and nitrated **cage 9**.[110] Notably, all of these cages demonstrated similar CO_2 adsorption capacities, measuring 47.8 cm^3 g^{-1} for **cage 4**, 45.8 cm^3 g^{-1} for **cage 7**, 46.3 cm^3 g^{-1} for **cage 8**, and 45.8 cm^3 g^{-1} for **cage 9** at 273 K and 1 bar. Under the same conditions, the cages exhibited similar CH_4 adsorption capacities, measuring 13.7 cm^3 g^{-1} for **cage 4**, 11.2 cm^3 g^{-1} for **cage 7**, 12.1 cm^3 g^{-1} for **cage 8**, and 12.0 cm^3 g^{-1} for **cage 9**. Of these cages, **cage 8** demonstrated the greatest selectivity for CO_2/CH_4, with a value of 28.5.

Yuan *et al.* recently reported on sp^2 carbon-linked POCs (**sp^2c-POCs**) that possess distinctive triangular prism structures through a one-step Knoevenagel reaction (Fig. 7).[111] The **sp^2c-POCs**

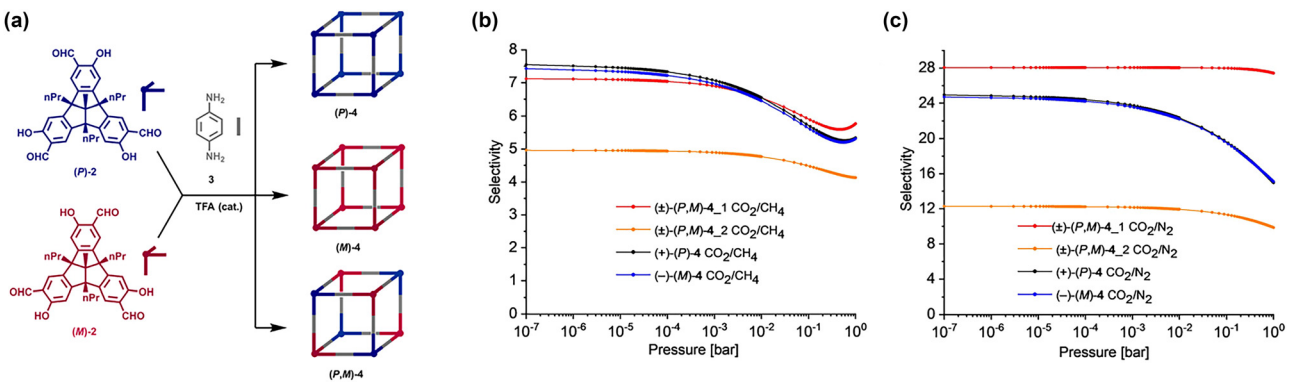

Fig. 6 (a) Condensation of the tri(salicylaldehyde) 2 with *p*-phenylenediamine 3 leading to the cubic [8+12] imine cage compounds **(P)-4**, **(M)-4** and **(P,M)-4**. The cage compounds are represented schematically as cubes with the TBTQ-units at their vertices in blue for the (*P*)-enantiomer, in red for the (*M*)-enantiomer and the linear *p*-phenylenediimine linkers at the edges in grey. (b) IAST selectivity curves of the [8+12] cage compounds for CO_2/CH_4 (50 : 50) at 273 K and (c) for CO_2/N_2 (20 : 80) at 273 K. Reproduced with permission from ref. 108. Copyright 2021, Wiley.

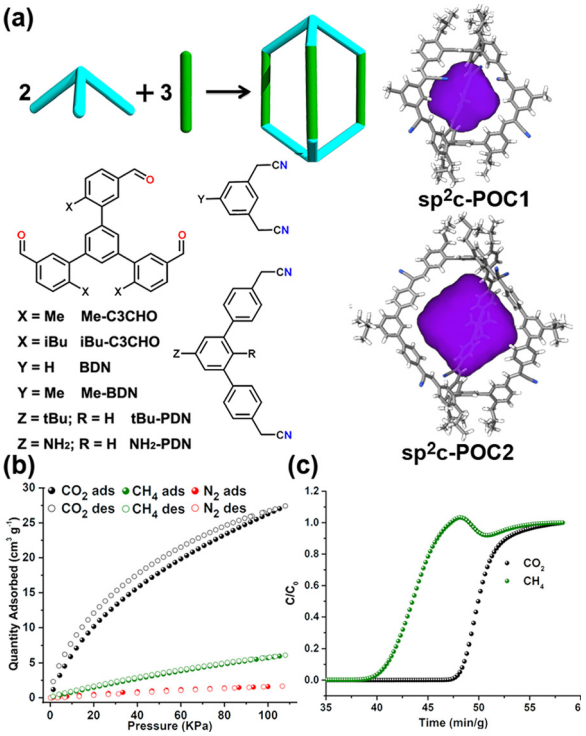

Fig. 7 (a) The synthetic route of [2+3] sp^2c-POCs and their single-crystal X-ray structures. (b) CO_2, CH_4 and N_2 adsorption isotherms of **sp^2c-POC1** at 298 K. (c) Experimental breakthrough curves of an equimolar mixture of CO_2/CH_4 at 298 K and 1 bar over a packed bed of **sp^2c-POC1**. Reproduced with permission from ref. 111. Copyright 2023, Chinese Chemical Society.

are highly stable, maintaining their structural integrity even in the presence of concentrated HCl, concentrated HNO_3, or saturated NaOH solutions. Notably, **sp^2c-POC1** has the highest BET surface area (350 m^2 g^{-1}) among all **sp^2c-POCs**. In addition, **sp^2c-POC1** can absorb 27.4 cm^3 g^{-1} of CO_2 and 6.1 cm^3 g^{-1} of CH_4, but has negligible affinity for N_2 at 298 K and 1 bar. The observed differences in gas uptake capacities imply that **sp^2c-POC1** can be useful in separating CO_2/N_2 and CO_2/CH_4 mixtures. The IAST selectivities of **sp^2c-POC1** were calculated, yielding values of 21 and 52 for CO_2/CH_4 (50 : 50) and CO_2/N_2 (15 : 85) mixtures, respectively. Breakthrough experiments have substantiated the excellent separation performance of **sp^2c-POC1** for CO_2/CH_4 and CO_2/N_2 gas mixtures. Moreover, the exceptional stability demonstrated by **sp^2c-POC1** highlights its potential as a solid adsorbent for purifying and separating natural and flue gases.

The separation of CO_2 and C_2H_2 is crucial in producing high-purity C_2H_2 by eliminating CO_2 impurities and poses significant challenges due to their similar molecular sizes and physical characteristics. It is imperative to study the gas sorption and separation behavior of CO_2 and C_2H_2 in POC with intrinsic porosity, abundant electron-rich π calix[4]-resorcinarene cavities, and oxygen and nitrogen sites. In 2021, Yuan *et al.* discovered a lantern-shaped calix[4]resorcinarene-based POC (**CPOC-101**) that exhibits eight distinct solvatomorphs when subjected to crystallization in different solvents,[93] presenting a significant breakthrough. Specifically, the **CPOC-101α** variant obtained through crystallization in toluene/chloroform demonstrated an apparent BET surface area of up to 406 m^2 g^{-1} as determined by nitrogen gas sorption at 77 K, which was much higher than other solvatomorphs of **CPOC-101** with BET surface area below 40 m^2 g^{-1}. Most importantly, the **CPOC-101α** variant showed superior adsorption capacities for C_2H_2 and CO_2 and greater ability in C_2H_2/CO_2 separation than **CPOC-101β**, which served as the representative solvatomorph with low BET surface areas. At 298 K and 1 bar, the activation of **CPOC-101α** resulted in adsorption capacities of CO_2 and C_2H_2 of up to 63 and 95 cm^3 g^{-1}, respectively, while **CPOC-101β** resulted in lower adsorption capacities of 39 and 60 cm^3 g^{-1} under the same conditions. At ambient conditions, dynamic breakthrough experiments were conducted to verify the practical separation performance of C_2H_2/CO_2 using **CPOC-101**. The longer separation time of **CPOC-101α** compared to **CPOC-101β** indicates that it has a higher preference for trapping C_2H_2 over CO_2. Calculating the separation factors of C_2H_2/CO_2 for **CPOC-101α** and **CPOC-101β** using breakthrough experiments yields values of 2.2 and 2.0, respectively. Additionally, the stability of **CPOC-101α** was confirmed through recycling experiments where the breakthrough time remained consistent after four cycles.

In 2017, Yuan *et al.* reported the synthesis of seven water-stable hydrazone-linked POCs with four distinct assembly modes: **HPOC-101**, **HPOC-102**, **HPOC-103**, and **HPOC-104**.[112] These cages were synthesized *via* coupling reaction between C4RACHO and various dihydrazides (Fig. 8). The characterization of the porous organic cages revealed calculated BET surface areas ranging from 373 to 563 m^2 g^{-1}. Additionally, the cages' adsorption properties towards CO_2 and C_2H_2 at room temperature were investigated, resulting in C_2H_2 capacities ranging from 31 to 47 cm^3 g^{-1} and CO_2 capacities ranging from 24 to 33 cm^3 g^{-1}. These cages notably exhibited a preference for C_2H_2 adsorption over CO_2. To assess their applicability in C_2H_2/CO_2 separation, breakthrough experiments using a C_2H_2/CO_2 mixture (50 : 50), were specifically conducted for **HPOC-102** and **HPOC-104**, which resulted in the effective separation of the C_2H_2/CO_2 mixture. These breakthrough experiments highlight the promising performance of the cages in C_2H_2/CO_2 separation. Furthermore, **HPOC-102** and **HPOC-104** serve as pioneering examples of hydrazone-linked POC materials successfully achieving C_2H_2/CO_2 gas separation.

2.2. Light hydrocarbon purification

The separation of light hydrocarbons into individual components with the desired purity remains a significant objective in the petrochemical industry. Cryogenic distillation, a prevailing method, is expensive and energy-intensive, leading to the emergence of adsorption separation with porous materials as a promising alternative technology. Recently, a few POCs have been synthesized to achieve highly efficient separation of light hydrocarbons.

In 2018, Mastalerz *et al.* reported the synthesis of a small series of [4+6] boronic ester cages that varied in the degrees of fluorine content within the diboronic ester struts.[113] Of the fluorinated cages, cages **10*** and **11*** exhibited noteworthy

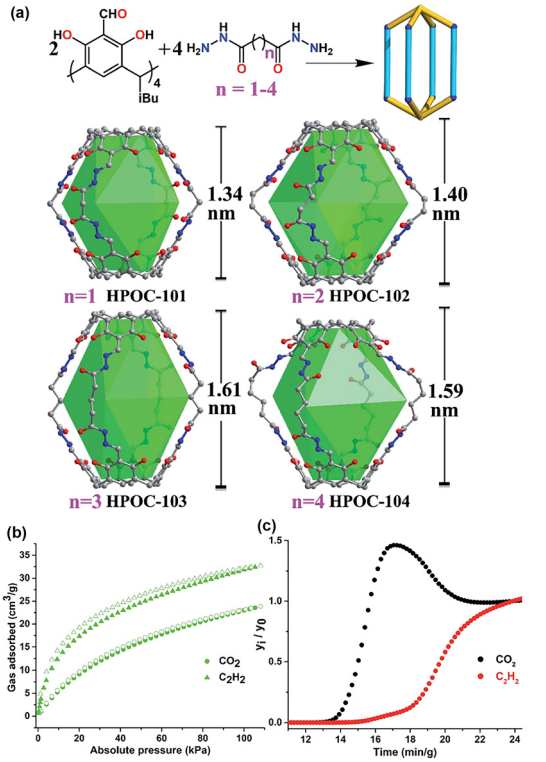

Fig. 8 (a) Schematic illustration of the assembly of [2+4] lanterns *via* hydrazone coupling of C4RACHO and alkanedihydrazides, along with their single-crystal X-ray structures and inner cavity heights. (b) CO_2 and C_2H_2 adsorption isotherms of **HPOC-102** at 298 K. (c) Experimental breakthrough curves of an equimolar mixture of CO_2/C_2H_2 at 298 K and 1 bar over a packed bed of **HPOC-102**. Reproduced with permission from ref. 112. Copyright 2021, Royal Society of Chemistry.

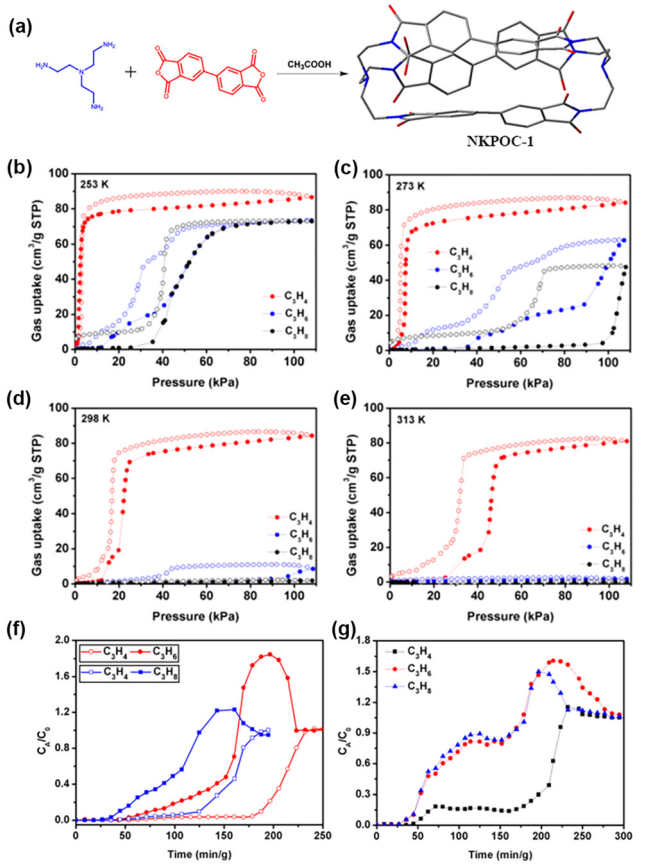

Fig. 9 (a) Synthesis of **NKPOC-1** (C, gray; N, blue; O, red). Sorption isotherms of **NKPOC-1-α** for C_3H_4, C_3H_6, and C_3H_8 at (b)253 K, (c) 273 K, (d) 298 K, and (e) 313 K. Filled and open symbols represent adsorption and desorption, respectively. (f) Dynamic experimental fixed-bed column breakthrough results of binary (2 : 1 v/v) C_3H_4/C_3H_6 and C_3H_4/C_3H_8 gas mixtures in an absorber bed packed with activated **NKPOC-1-α**. (g) Ternary breakthrough experiment for a $C_3H_4/C_3H_6/C_3H_8$ (2 : 1 : 1 v/v/v) gas mixture. Reproduced with permission from ref. 91. Copyright 2019, American Chemical Society.

properties. Notably, non-fluorinated **cage 9*** had an excellent specific surface area of 511 $m^2\ g^{-1}$. Encouraged by this result, subsequent investigations concentrated on the adsorption and separation performance of **cage 9*** for small hydrocarbons. The gas adsorption capacity of **cage 9*** was found to be 2.52 mmol g^{-1} for C_2H_6, 2.50 mmol g^{-1} for C_2H_4, and 2.53 mmol g^{-1} for C_2H_2. The selectivities for C_2H_6/C_2H_4, C_2H_6/C_2H_2, and C_2H_4/C_2H_2 based on a hypothetical 1 : 1 mixture were evaluated to be 1.29, 1.52, and 1.17, respectively.

Zhang *et al.* subsequently reported the synthesis of a new class of soft porous crystals utilizing an [2+3] imide-based organic cage referred to as **NKPOC-1** (Fig. 9).[91] One intriguing characteristic of **NKPOC-1** is its guest-induced breathing behavior, where it undergoes reversible transformations from a "closed" nonporous phase (α) to two distinct porous "open" phases (β and γ) upon exposure to various gas molecules. Notably, **NKPOC-1-α** exhibits remarkable selectivity for propyne (C_3H_4) adsorption over propylene (C_3H_6) and propane (C_3H_8) under ambient conditions. To evaluate its separation capabilities, dynamic breakthrough experiments were conducted using binary and ternary gas mixtures consisting of C_3H_4/C_3H_6 (2 : 1, v/v), C_3H_4/C_3H_8 (2 : 1, v/v), and $C_3H_4/C_3H_6/C_3H_8$ (2 : 1 : 1, v/v/v) at 298 K. **NKPOC-1-α** demonstrates exceptional separation efficiency in the case of binary C_3H_4/C_3H_6 and C_3H_4/C_3H_8 gas mixtures, with C_3H_4 saturation uptakes and breakthrough retention times of 75.6 $cm^3\ g^{-1}$ and 137 min g^{-1}, as well as 55.2 $cm^3\ g^{-1}$ and 100 min g^{-1}, respectively. Noteworthy, **NKPOC-1-α** also effectively removes C_3H_4 from a ternary gas mixture ($C_3H_4/C_3H_6/C_3H_8$, 2 : 1 : 1, v/v/v) under ambient conditions, based on a C_3H_4 retention duration of 135 min g^{-1} and a calculated C_3H_4 saturation uptake of 67 $cm^3\ g^{-1}$. This outstanding separation performance of **NKPOC-1-α** is attributed to its selective gate-opening effect for C3 hydrocarbons combined with the strength of the interactions once the gate is open.

Yuan *et al.* identified a promising POC, known as **CPOC-301**, which is composed of a highly porous [6+12] octahedral calix[4]resorcinarene structure (Fig. 10).[92] It is important that **CPOC-301** shows exceptional ability in selectively capturing C_2H_6 from mixtures with C_2H_4, resulting in the direct production of high-purity C_2H_4. **CPOC-301** can adsorb up to 670 $cm^3\ g^{-1}$ of N_2, a maximal capacity that corresponds to a calculated BET surface area of 1962 $m^2\ g^{-1}$. A key finding is that, at 293 K, **CPOC-301** selectively binds C_2H_6 more strongly (87 $cm^3\ g^{-1}$) than C_2H_4 (75 $cm^3\ g^{-1}$). The researchers calculated that the heat of adsorption

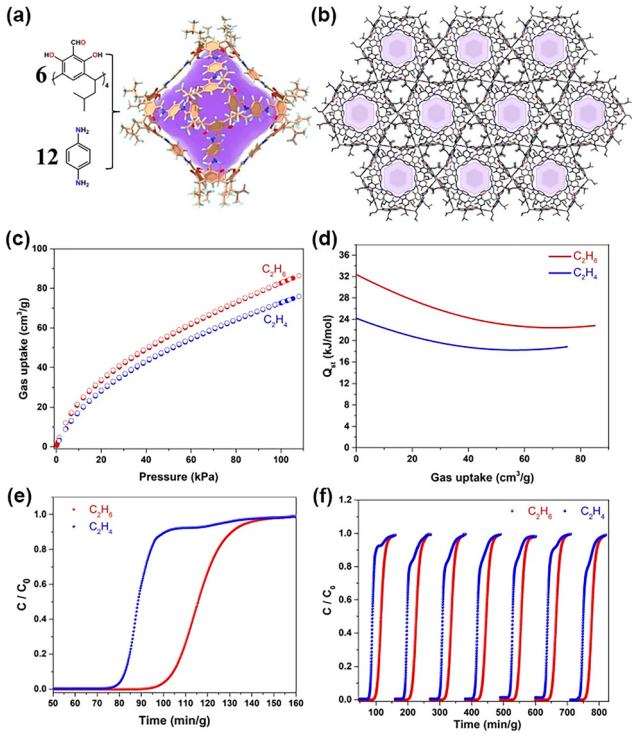

Fig. 10 (a) The X-ray crystal structure of **CPOC-301**. (b) The Solid-state molecular packing of **CPOC-301** viewed from [001] direction, where H atoms are committed for clarity. Color codes: phenyl ring; orange, carbon; gray, oxygen; red, nitrogen; blue, and hydrogen; light turquoise. (c) Experimental C_2H_6 and C_2H_4 adsorption isotherms of **CPOC-301** at 293 K. (d) Isosteric heat of adsorption plots for the adsorption of C_2H_6 and C_2H_4 by **CPOC-301**. (e) Experimental breakthrough curves for equimolar mixture of C_2H_6/C_2H_4 at 298 K and 1 bar over a packed bed of **CPOC-301**. (f) The recyclability of **CPOC-301** under multiple mixed gas column breakthrough tests. Reproduced with permission from ref. 92. Copyright 2021, Springer Nature.

(Q_{st}) at zero coverage for C_2H_6 and C_2H_4 is 32.4 and 24.2 kJ mol^{-1}, respectively. This observation suggests that the host–guest interactions between **CPOC-301** and C_2H_6 are much stronger than those with C_2H_4. The researchers attribute the stronger attraction of **CPOC-301** to C_2H_6 as a result of the creation of multiple C–H···π hydrogen bonds between C_2H_6 and the resorcin[4]arene cavities, demonstrated by first-principles dispersion-corrected density functional theory (DFT-D) calculations. Additionally, breakthrough experiments have validated the efficient isolation of C_2H_4 from C_2H_6/C_2H_4 mixtures using **CPOC-301**. The researchers provide the calculated separation factor for an equimolar mixture of C_2H_6/C_2H_4, which is 1.3, a value that aligns well with the predicted IAST value. Further, researchers found that the **CPOC-301** consistently maintains its separation performance over seven consecutive cycles, which demonstrates its robustness and positions it as a promising candidate for C_2H_4 purification purposes.

Recently, Yuan *et al.* explored the functionalities of the octahedral calix[4]resorcinarene-based hydrazone-linked porous organic cage (**HPOC-401**) as a prototype for post-synthetic metalation with different transition metal ions.[114] The study demonstrated that **HPOC-401** has exceptional properties for this purpose, even under mild conditions. The BET surface areas of **HPOC-401** after being metalated with various transition metal ions, namely **HPOC-401-V**, **HPOC-401-Cu**, **HPOC-401-Zn**, and **HPOC-401-Mo**, were significantly increased compared to pristine **HPOC-401**. The specific surface areas measured were 1456 $m^2 g^{-1}$ (**HPOC-401-V**), 1099 $m^2 g^{-1}$ (**HPOC-401-Cu**), 983 $m^2 g^{-1}$ (**HPOC-401-Zn**), and 710 $m^2 g^{-1}$ (**HPOC-401-Mo**), while **HPOC-401** had a surface area of 474 $m^2 g^{-1}$. Furthermore, the metalated **HPOC-401** showed enhanced CO_2, H_2, and C2 hydrocarbon uptake capacity along with improved selectivity for C_2H_6/C_2H_4, compared to the pure **HPOC-401**. Specifically, **HPOC-401-V** and **HPOC-401-Cu** displayed an interesting preference for C_2H_6 over C_2H_4. However, **HPOC-401** alone does not exhibit selective adsorption of C_2H_6. Remarkably, **HPOC-401-V** demonstrated an outstanding C_2H_6/C_2H_4 selectivity of up to 2.3, which surpasses the selectivity values of other POCs. The breakthrough results indicate the potential of **HPOC-401-V** to achieve efficient one-step separation of C_2H_4 from an equimolar mixture of C_2H_6/C_2H_4.

2.3. Separation for Xe/Kr rare gases

Noble gases, including Kr and Xe, are widely used in diverse industries such as gas lasers, semiconductor, photography lighting, and medical fields.[115] However, unstable and hazardous radioisotopes of Kr and Xe, like ^{133}Xe and ^{85}Kr, can be generated by used nuclear fuel reprocessing facilities or nuclear accidents. When these radioisotopes escape into the atmosphere, they pose risks to the environment and living organisms.

Cooper *et al.* developed the first reported POC material for Xe/Kr separation with exceptional performance (Fig. 11).[88] The team used a [4+6] tetrahedral POC called **CC3**, which is an imine-linked structure formed by the Schiff-base reaction of 1,3,5-triformylbenzene and 1,2-diaminocyclohexane in a 2 : 3 molar ratio. **CC3** was chosen primarily because the largest inclusion sphere in the **CC3** cavity measures 4.4 Å, which is close to the size of Xe (4.10 Å). Notably, the window diameter of **CC3** observed in its static solid-state crystal structure is only 3.6 Å, which is theoretically too narrow to allow for Xe and Kr diffusion, with diameters of 4.10 Å and 3.69 Å, respectively. However, the flexibility of the cage structure, attributed to cage vibrations, results in temporary enlargement of the pore diameter. Despite being relatively soft since **CC3** is assembled from discrete molecules, it exhibits structural deformations, such as window vibrations and packing changes under certain temperature and pressure conditions, allowing many gas molecules to access the pores of **CC3**. The simulations and experimental gas adsorption isotherms and molecular dynamics revealed that **CC3** can accommodate both Xe and Kr, and it demonstrated a strong Xe preferential adsorption over Kr, as evidenced by calculations of the isosteric heat of adsorption. The calculated Xe/Kr selectivity for **CC3** reached a value of 20.4, surpassing many MOF materials. To examine the practical separation performance of rare gases at low concentrations in the air, mimicking the spent nuclear fuels reprocessing, the researchers conducted experimental breakthrough measurements. They used gas mixtures containing Xe (400 ppm), Kr (40 ppm), and other elements of air (N_2, O_2, and CO_2), which were passed through a packed column of **CC3** crystals. The Kr

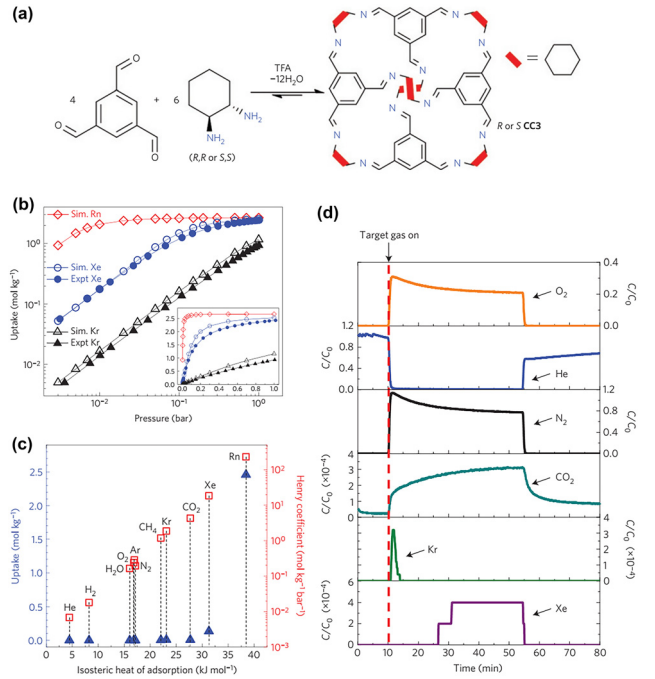

Fig. 11 (a) Schematic illustration of the assembly of **CC3**. (b) Predicted and experimental single-component gas adsorption isotherms for **CC3** at 298 K. (c) Isosteric heat of adsorption calculations of noble and other gases at 298 K. (d) Breakthrough curves for **CC3** by Xe, Kr, and common gas mixtures. Reproduced with permission from ref. 88. Copyright 2014, Springer Nature.

gas was immediately detected in the effluent, while Xe gas was retained for more than 15 min, which is consistent with the observation of stronger host–guest interactions between Xe and the cage relative to Kr.

In 2016, Thallapally *et al.* reported the selective uptake of Xe by two previously reported POCs,[116] namely **noria** and **PgC-noria**. These POCs were prepared with an acid-catalyzed condensation reaction between glutaraldehyde and resorcinol (for **noria**) and pyrogallic acid (for **PgC-noria**), in the presence of concentrated hydrochloric acid. The isotherms for Xe and Kr adsorption were measured for both **noria** and **PgC-noria**. It was observed that both POCs showed selectivity towards Xe over Kr, with **noria** demonstrating greater Xe adsorption compared to **PgC-noria**. Furthermore, the IAST calculations demonstrated that **noria** displayed an exceptional Xe/Kr selectivity of 9.4 under dilute conditions. The remarkable Xe/Kr selectivity, coupled with the high thermal stability of **noria** implies that it could be a promising candidate for capturing Xe from the off-gas produced during the reprocessing of used nuclear fuel.

2.4. Separation for fluorinated greenhouse gases

Manufactured fluorinated gases, including SF_6, perfluorocarbons (PFCs), and nitrogen trifluoride (NF_3), are widely utilized in modern industries such as refrigerants, propellants, and blowing agents.[117–119] However, it is important to note that fluorinated gases are highly toxic and potent greenhouse gases whose global warming potentials are thousands of times higher than that of CO_2. Therefore, the development of porous adsorbents for selective adsorption of fluorinated gases, prioritizing them over other less harmful gases, is critical in both industrial and environmental domains. POCs have undergone development for the separation of fluorinated gases.

In 2016, Cooper *et al.* investigated whether four [4+6] imine-linked tetrahedral POCs (**CC2**, **CC3**, **CC5**, and **CC13**) could be potentially applied to separate SF_6 from N_2.[89] These POCs were synthesized through a Schiff-base reaction between diamine and tri-aldehyde in a 3 : 2 molar ratio. Adsorption experiments were conducted to evaluate their capability for SF_6 gas uptake, revealing that all four cages demonstrated SF_6 adsorption but at varying capacities due to their structural differences. It is important to note that the kinetic diameter of SF_6 (5.5 Å) exceeds the window diameters (~3.6 Å) of **CC2**, **CC3**, and **CC13**, suggesting that they are not capable of encapsulating SF_6. However, these POCs possess a flexible nature that enables them to adsorb SF_6 despite its larger size than the static window diameter. Further analysis of the adsorption isotherms indicated that **CC3α** exhibited a typical type I adsorption behavior characterized by sharp increases at low pressures, indicating its higher affinity for SF_6. This finding was supported by the calculated Q_{st} values. Furthermore, **CC3** showed the highest SF_6/N_2 selectivity among the four POCs, and activated **CC3α** achieved selectivities of 178 at 273 K and 74 at 298 K for a 10 : 90 SF_6:N_2 mixture, which exceeds those of many reported MOFs. Additional simulations suggested that cooperative diffusion and structural rearrangements within **CC3** contribute to the near-ideal behavior of the host for SF_6 guest molecules. X-ray crystallography analysis provided insight into the location of SF_6 within the **CC3** cavity, confirming the strong interaction between the **CC3** host and SF_6 guest.

In 2022, Mastalerz *et al.* reported three isostructural [2+3] lantern-shaped POCs, including **H-cage** (with non-fluorinated *n*-butyl chains), **HF-cage** (with partially fluorinated *n*-butyl chains), and **F-cage** (with perfluorinated *n*-butyl chains), all with varying degrees of fluorinated side-chains (Fig. 12).[94] Triamino triptycene and terphenyl-based bis-salicylaldehydes were used in a 2 : 3 molar ratio, catalyzed by trifluoroacetic acid to construct these POCs. The gas adsorption behavior of fluorinated and non-fluorinated alkanes was compared among these isomorphic crystalline states to evaluate the impact of different side chains on gas sorption properties. The study showed that the fluorinated POCs preferentially adsorbed fluorinated gases, whereas the non-fluorinated POCs demonstrated a preference for non-fluorinated gases. Specifically, **F-cage** exhibited the highest uptakes of PFCs, such as tetrafluoromethane (CF_4), hexafluoroethane (C_2F_6), and octafluoropropane (C_3F_8), compared to the other two POCs. IAST selectivities of CF_4/N_2, C_2F_6/N_2, and C_3F_8/N_2 were calculated under different compositions and conditions (273 K and 1 bar), indicating that **F-cage** had a high selectivity for fluorinated gases over N_2. Additionally, **F-cage** showed the highest selectivity for fluorinated alkanes over non-fluorinated alkanes. Given its advantageous selective adsorption of PFCs, the researchers further investigated the sorption of octafluorocyclobutane

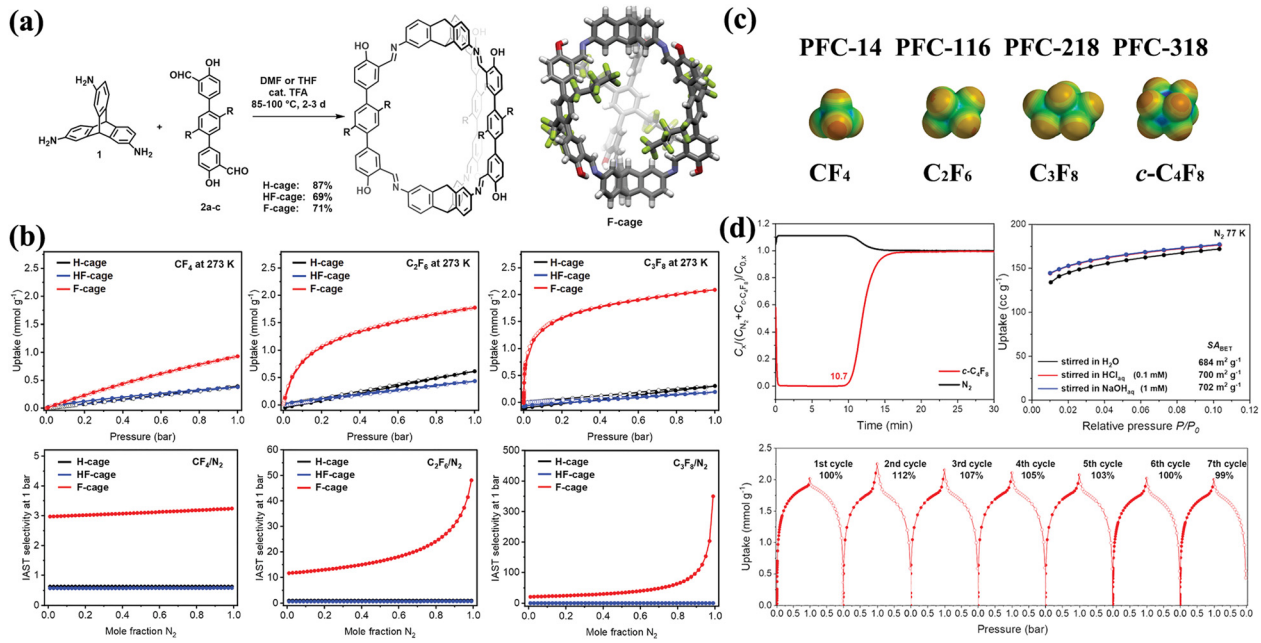

Fig. 12 (a) Synthesis of **H-cage**, **HF-cage**, and **F-cage** by imine condensation reactions of triamino triptycene and terphenyl bis-salicylaldehydes, and the single-crystal X-ray structure of **F-cage**. (b) PFC sorption properties of **H-cage**, **HF-cage**, and **F-cage** in comparison. (c) Space filling models of the fluorinated alkanes, including tetrafluoromethane (PFC-14), hexafluoroethane (PFC-116), octafluoropropane (PFC-218), and octafluorocyclobutane (PFC-318). (d) Applicability investigations of **F-cage**, including breakthrough curves and stablity tests. Reproduced with permission from ref. 94. Copyright 2022, Wiley.

(c-C_4F_8 or PFC-318) in more detail. **F-cage** demonstrated selectivity for c-C_4F_8/N_2 up to 41475. Experimental breakthrough analyses revealed that **F-cage** effectively separated c-C_4F_8 from N_2 mixtures with a breakthrough time of 107 minutes, and its separation performance remained consistent over seven consecutive cycles. Furthermore, F-cage demonstrated stability in neutral, acidic, and basic aqueous media as confirmed by ^1H and ^{19}F NMR spectroscopy, thermogravimetric analysis (TGA), and N_2 sorption at 77 K, indicating that **F-cage** is robust enough for real-world applications.

2.5. Separation for D_2/H_2 gas isotopes

Deuterium is an irreplaceable raw material that finds widespread use in scientific research, including isotope tracing, neutron scattering, and proton nuclear magnetic resonance spectroscopy, as well as industrial applications, such as fuel in nuclear fusion reactors and for fusion reactions, and in medical uses like imaging and cancer therapy. To meet the growing global demand for deuterium, the development of a cost-effective and large-scale separation method is crucial. Two approaches for separating hydrogen isotopes using porous materials are kinetic quantum sieving (KQS), which utilizes nanoconfined space, and chemical affinity quantum sieving (CAQS), which relies on strong metal adsorption sites. Various porous materials, including activated carbons, zeolites, MOFs, and COFs, have been investigated in attempts to separate D_2 from H_2.[120–127] However, the selectivity of D_2/H_2 using these materials is often low, typically less than 2, for both separation strategies. Porous materials with ultra-fine pore apertures (~3 Å) are critical for achieving KQS but are challenging to obtain in activated carbons, zeolites, MOFs, and COFs.

Cooper *et al.* utilized PSM synthesis in 2019, which proved to be effective in modifying POCs' internal cavities and fine-tuning the pore sizes, resulting in outstanding quantum sieves.[90] Their work produced six internal functionalized POCs, namely **6ET-RCC3**, **1PT-5FT-RCC3**, **1AT-5FT-RCC3**, **1ET-5FT-RCC3**, **5FT-RCC3**, and **6FT-RCC3**, with PLE values ranging from 1.95 Å to 3.50 Å (Fig. 13). To achieve this, a post-synthetic "tying" and protection-deprotection strategy were utilized based on **RCC3**, a reduced derivative of **CC3**. The POCs demonstrated a trade-off behavior, where those with lower PLE values exhibited lower D_2 adsorption capacities but higher selectivity while conversely, those with higher PLE values exhibited high D_2 adsorption capacities and lower selectivity. The upscaling of the internal functionalized POCs for practical applications presented significant challenges. Nonetheless, combining the small-pore and large-pore functionalized POCs through cocrystallization into a single solid resulted in a material with optimal separation performance, exhibiting excellent D_2/H_2 selectivity (8.0) and high deuterium uptake (4.7 mmol g^{-1}). In 2022, Vogel *et al.* used *ab initio* molecular dynamics (AIMD) simulations to explain how the internal functionalized POCs could manage D_2 and H_2 separation, leading to the targeted design of novel porous adsorbents for hydrogen isotope separation.[128]

3. Conclusions

In summary, numerous POCs of different shapes, sizes, and functions have been designed and synthesized in the last

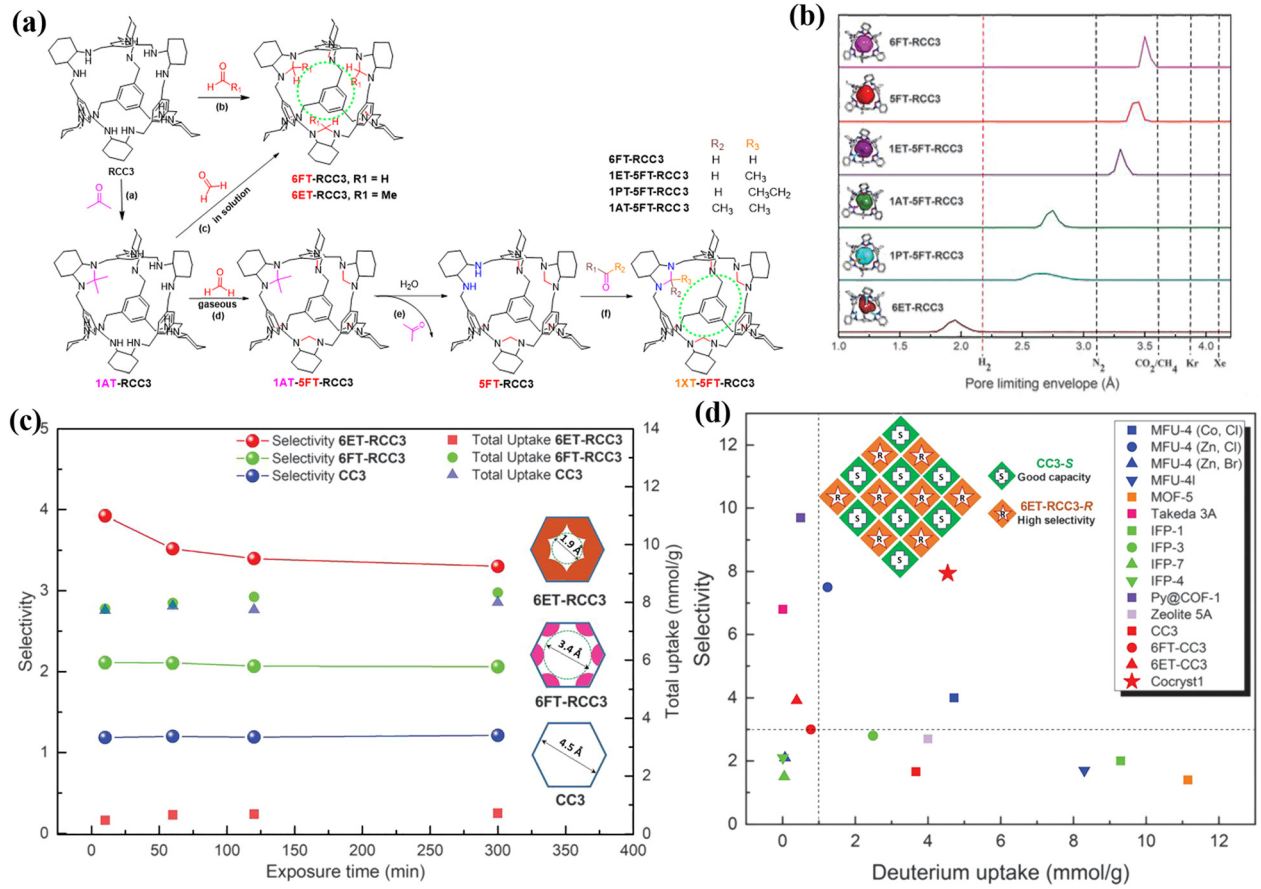

Fig. 13 (a) Full synthesis route for the internal functionalized POCs (including **6ET-RCC3**, **1PT-5FT-RCC3**, **1AT-5FT-RCC3**, **1ET-5FT-RCC3**, **5FT-RCC3**, and **6FT-RCC3**). (b) Representative single-crystal structures of the modified cages showing accessible cavities (colored), along with calculated PLEs for each system. (c) D_2/H_2 selectivities and gas uptakes as a function of exposure time at 30 K for **CC3**, **6FT-RCC3**, and **6ET-RCC3**. (d) Summary of hydrogen isotope KQS selectivities and adsorption capacities for various porous materials. Reproduced with permission from ref. 90. Copyright 2019, American Association for the Advancement of Science.

decade utilizing various organic synthons and covalent condensation reactions. However, only a few of these have been explored for gas separation. To our knowledge, POCs have only been examined in specific gas separation systems such as CO_2/N_2, CO_2/CH_4, C_2H_2/CO_2, rare gases Xe/Kr, greenhouse SF_6/N_2, isotope separation D_2/H_2, and separation of industrially important C2 and C3 hydrocarbons through mixed gas experiments. These instances have been reviewed thoroughly. However, the gas separation applications of POCs are still in the early stage, and their uses have been limited to the aforementioned gas components in mixed gas experiments. Herein, we present some essential perspectives on the potential applications of POCs in gas separation.

(1) Developing stable POCs

Although many POCs have been assembled using dynamically reversible imine and boronate ester bonds, these components are sensitive to hydrolysis under acid, base, or even moisture conditions. This sensitivity often leads to POCs' decomposition, significantly hindering their practical use in gas separation studies considering the presence of acidic, basic, or water vapor gases in gas mixtures. Thus, there is a high demand for the development of robust covalent linkages to build chemically stable POCs using simple and cost-effective procedures.[111]

(2) Separation of industrially important gases and multi-component gas mixtures

POCs exhibit potential for exploring the applications of separating industrially important C4–C6 hydrocarbons as well as multi-component gas mixtures.[129–131] POCs may exhibit unexpected and unique separation behavior compared to other extensively studied porous materials such as MOFs, zeolites, and POPs. "Soft" porous materials with flexible and adaptive pore structures have gained attention in recent years because of their capacity to adjust their structures to control gas mobility and diffusivity in their pores for efficient purification.[132–134] POCs possess the inherent attribute to serve as "soft" porous materials. They are constructed from small molecules that interact weakly in the solid-state,[39,94] allowing gas guests to gain pore access *via* structural deformations under specified conditions.

(3) Efficient and precise separation

Due to their discrete molecules, POCs can be designed with finely-tuned pore sizes at a remarkably precise level with

selective interior functionalization. This level of control is challenging to achieve in other porous materials such as COFs and MOFs. Commonly, the strategy of tuning pores in MOFs and COFs involves systematically expanding or reducing the number of phenylene rings in the organic linker, resulting in coarse tuning increments or decrements of approximately 2.8 Å. This tuning method is not suitable for achieving fine-tuning of pores. Therefore, POCs have the potential to achieve high selectivity for the separation of gas mixtures with similar molecule shapes by designing appropriate pores through a fine-tuning approach. This fine-tuning method maintains high gas adsorption capacity while also maintaining the nearly unchanged original cavities.

(4) Gas separation using POC-based membranes

Membrane technology has emerged as an efficient and energy-saving alternative for gas separation and purification processes. Leveraging the advantageous solubility and solvent processability of POCs, researchers have successfully developed pure POC-based membranes and mixed matrix membranes. These innovative membranes have demonstrated significant potential across various applications involving gases, ions and small organic molecules.[135–138] Therefore, it is imperative to emphasize the promising prospect of achieving high-performance membranes by precisely controlling both the intrinsic and extrinsic pores of POCs.

Conflicts of interest

There are no conflicts to declare.

Acknowledgements

This work was financially supported by the National Nature Science Foundation of China (22071244, 22275191, 22275186), Youth Innovation Promotion Association CAS (2022305), Fujian Science & Technology Innovation Laboratory for Optoelectronic Information of China (2021ZZ106) and Natural Science Foundation of Fujian Province of China (2022J01503).

References

1 D. S. Sholl and R. P. Lively, Seven chemical separations to change the world, *Nature*, 2016, **532**, 435–437.
2 N. A. Downie, *Industrial gases*, Springer Science & *Business Media*, 2007.
3 R. Faiz and K. Li, Olefin/paraffin separation using membrane based facilitated transport/chemical absorption techniques, *Chem. Eng. Sci.*, 2012, **73**, 261–284.
4 M. Shen, L. Tong, S. Yin, C. Liu, L. Wang, W. Feng and Y. Ding, Cryogenic technology progress for CO_2 capture under carbon neutrality goals: A review, *Sep. Purif. Technol.*, 2022, **299**, 121734.
5 A. Ebadi Amooghin, H. Sanaeepur, R. Luque, H. Garcia and B. Chen, Fluorinated metal-organic frameworks for gas separation, *Chem. Soc. Rev.*, 2022, **51**, 7427–7508.
6 J.-R. Li, R. J. Kuppler and H.-C. Zhou, Selective gas adsorption and separation in metal-organic frameworks, *Chem. Soc. Rev.*, 2009, **38**, 1477–1504.
7 K. Adil, Y. Belmabkhout, R. S. Pillai, A. Cadiau, P. M. Bhatt, A. H. Assen, G. Maurin and M. Eddaoudi, Gas/vapour separation using ultra-microporous metal-organic frameworks: Insights into the structure/separation relationship, *Chem. Soc. Rev.*, 2017, **46**, 3402–3430.
8 I. C. Medeiros-Costa, E. Dib, N. Nesterenko, J.-P. Dath, J.-P. Gilson and S. Mintova, Silanol defect engineering and healing in zeolites: Opportunities to fine-tune their properties and performances, *Chem. Soc. Rev.*, 2021, **50**, 11156–11179.
9 Y.-X. Tan, F. Wang and J. Zhang, Design and synthesis of multifunctional metal-organic zeolites, *Chem. Soc. Rev.*, 2018, **47**, 2130–2144.
10 T. Lan, L. Li, Y. Chen, X. Wang, J. Yang and J. Li, Opportunities and critical factors of porous metal–organic frameworks for industrial light olefins separation, *Mater. Chem. Front.*, 2020, **4**, 1954–1984.
11 S. Zhang, M. K. Taylor, L. Jiang, H. Ren and G. Zhu, Light hydrocarbon separations using porous organic framework materials, *Chem. – Eur. J.*, 2020, **26**, 3205–3221.
12 J.-S. M. Lee and A. I. Cooper, Advances in conjugated microporous polymers, *Chem. Rev.*, 2020, **120**, 2171–2214.
13 S. Das, P. Heasman, T. Ben and S. Qiu, Porous organic materials: Strategic design and structure-function correlation, *Chem. Rev.*, 2017, **117**, 1515–1563.
14 F. Jin, E. Lin, T. Wang, S. Geng, T. Wang, W. Liu, F. Xiong, Z. Wang, Y. Chen, P. Cheng and Z. Zhang, Bottom-up synthesis of 8-connected three-dimensional covalent organic frameworks for highly efficient ethylene/ethane separation, *J. Am. Chem. Soc.*, 2022, **144**, 5643–5652.
15 Z. Zhang, C. Kang, S. B. Peh, D. Shi, F. Yang, Q. Liu and D. Zhao, Efficient adsorption of acetylene over CO_2 in bioinspired covalent organic frameworks, *J. Am. Chem. Soc.*, 2022, **144**, 14992–14996.
16 C. He, Y. Wang, Y. Chen, X. Wang, J. Yang, L. Li and J. Li, Microregulation of pore channels in covalent-organic frameworks used for the selective and efficient separation of ethane, *ACS Appl. Mater. Interfaces*, 2020, **12**, 52819–52825.
17 Y. Zhou, C. Chen, R. Krishna, Z. Ji, D. Yuan and M. Wu, Tuning pore polarization to boost ethane/ethylene separation performance in hydrogen-bonded organic frameworks, *Angew. Chem., Int. Ed.*, 2023, **62**, e202305041.
18 R.-B. Lin, Y. He, P. Li, H. Wang, W. Zhou and B. Chen, Multifunctional porous hydrogen-bonded organic framework materials, *Chem. Soc. Rev.*, 2019, **48**, 1362–1389.
19 Y. Yang, L. Li, R.-B. Lin, Y. Ye, Z. Yao, L. Yang, F. Xiang, S. Chen, Z. Zhang, S. Xiang and B. Chen, Ethylene/ethane separation in a stable hydrogen-bonded organic framework through a gating mechanism, *Nat. Chem.*, 2021, **13**, 933–942.
20 X. Yang, Z. Ullah, J. F. Stoddart and C. T. Yavuz, Porous organic cages, *Chem. Rev.*, 2023, **123**, 4602–4634.

21 E. J. Gosselin, C. A. Rowland and E. D. Bloch, Permanently microporous metal-organic polyhedra, *Chem. Rev.*, 2020, **120**, 8987–9014.
22 A. Schoedel, Z. Ji and O. M. Yaghi, The role of metal-organic frameworks in a carbon-neutral energy cycle, *Nat. Energy*, 2016, **1**, 16034.
23 E. González-Zamora and I. A. Ibarra, CO_2 capture under humid conditions in metal–organic frameworks, *Mater. Chem. Front.*, 2017, **1**, 1471–1484.
24 T. Wang, E. Lin, Y.-L. Peng, Y. Chen, P. Cheng and Z. Zhang, Rational design and synthesis of ultramicroporous metal-organic frameworks for gas separation, *Coord. Chem. Rev.*, 2020, **423**, 213485.
25 Y. Wang, W. Liu, Z. Bai, T. Zheng, M. A. Silver, Y. Li, Y. Wang, X. Wang, J. Diwu, Z. Chai and S. Wang, Employing an unsaturated Th^{4+} site in a porous thorium-organic framework for Kr/Xe uptake and separation, *Angew. Chem., Int. Ed.*, 2018, **57**, 5783–5787.
26 I. Weinrauch, I. Savchenko, D. Denysenko, S. M. Souliou, H. H. Kim, M. Le Tacon, L. L. Daemen, Y. Cheng, A. Mavrandonakis, A. J. Ramirez-Cuesta, D. Volkmer, G. Schuetz, M. Hirscher and T. Heine, Capture of heavy hydrogen isotopes in a metal-organic framework with active Cu(I) sites, *Nat. Commun.*, 2017, **8**, 14496.
27 T. Hasell and A. I. Cooper, Porous organic cages: Soluble, modular and molecular pores, *Nat. Rev. Mater.*, 2016, **1**, 16053.
28 K. Acharyya and P. S. Mukherjee, Organic imine cages: Molecular marriage and applications, *Angew. Chem., Int. Ed.*, 2019, **58**, 8640–8653.
29 M. Mastalerz, Porous shape-persistent organic cage compounds of different size, geometry, and function, *Acc. Chem. Res.*, 2018, **51**, 2411–2422.
30 R. D. Mukhopadhyay, Y. Kim, J. Koo and K. Kim, Porphyrin boxes, *Acc. Chem. Res.*, 2018, **51**, 2730–2738.
31 F. Wang, C. Bucher, Q. He, A. Jana and J. L. Sessler, Oligopyrrolic cages: From classic molecular constructs to chemically responsive polytopic receptors, *Acc. Chem. Res.*, 2022, **55**, 1646–1658.
32 S. Huang, Z. Lei, Y. Jin and W. Zhang, By-design molecular architectures via alkyne metathesis, *Chem. Sci.*, 2021, **12**, 9591–9606.
33 F. Beuerle and B. Gole, Covalent organic frameworks and cage compounds: Design and applications of polymeric and discrete organic scaffolds, *Angew. Chem., Int. Ed.*, 2018, **57**, 4850–4878.
34 T. Kunde, T. Pausch and B. M. Schmidt, Porous organic compounds - small pores on the rise, *Eur. J. Org. Chem.*, 2021, 5844–5856.
35 Q. Song, S. Jiang, T. Hasell, M. Liu, S. Sun, A. K. Cheetham, E. Sivaniah and A. I. Cooper, Porous organic cage thin films and molecular-sieving membranes, *Adv. Mater.*, 2016, **28**, 2629–2637.
36 T. Hasell, H. Zhang and A. I. Cooper, Solution-processable molecular cage micropores for hierarchically porous materials, *Adv. Mater.*, 2012, **24**, 5732–5737.
37 G. Zhu, F. Zhang, M. P. Rivera, X. Hu, G. Zhang, C. W. Jones and R. P. Lively, Molecularly mixed composite membranes for advanced separation processes, *Angew. Chem., Int. Ed.*, 2019, **58**, 2638–2643.
38 G. Zhu, D. O'Nolan and R. P. Lively, Molecularly mixed composite membranes: Challenges and opportunities, *Chem. – Eur. J.*, 2020, **26**, 3464–3473.
39 M. A. Little and A. I. Cooper, The chemistry of porous organic molecular materials, *Adv. Funct. Mater.*, 2020, **30**, 1909842.
40 T. Hasell, J. L. Culshaw, S. Y. Chong, M. Schmidtmann, M. A. Little, K. E. Jelfs, E. O. Pyzer-Knapp, H. Shepherd, D. J. Adams, G. M. Day and A. I. Cooper, Controlling the crystallization of porous organic cages: Molecular analogs of isoreticular frameworks using shape-specific directing solvents, *J. Am. Chem. Soc.*, 2014, **136**, 1438–1448.
41 M. Liu, M. A. Little, K. E. Jelfs, J. T. A. Jones, M. Schmidtmann, S. Y. Chong, T. Hasell and A. I. Cooper, Acid- and base-stable porous organic cages: Shape persistence and ph stability *via* post-synthetic "tying" of a flexible amine cage, *J. Am. Chem. Soc.*, 2014, **136**, 7583–7586.
42 H. Wang, Y. Jin, N. Sun, W. Zhang and J. Jiang, Post-synthetic modification of porous organic cages, *Chem. Soc. Rev.*, 2021, **50**, 8874–8886.
43 B. Dietrich, J. Lehn and J. Sauvage, Diaza-polyoxa-macrocycles and macrobicycles, *Tetrahedron Lett.*, 1969, **10**, 2885–2888.
44 T. Tozawa, J. T. A. Jones, S. I. Swamy, S. Jiang, D. J. Adams, S. Shakespeare, R. Clowes, D. Bradshaw, T. Hasell, S. Y. Chong, C. Tang, S. Thompson, J. Parker, A. Trewin, J. Bacsa, A. M. Z. Slawin, A. Steiner and A. I. Cooper, Porous organic cages, *Nat. Mater.*, 2009, **8**, 973–978.
45 T. Kunde, E. Nieland, H. V. Schroder, C. A. Schalley and B. M. Schmidt, A porous fluorinated organic [4+4] imine cage showing CO_2 and H_2 adsorption, *Chem. Commun.*, 2020, **56**, 4761–4764.
46 H. Duan, F. Cao, H. Hao, H. Bian and L. Cao, Efficient photoinduced energy and electron transfers in a tetraphenylethene-based octacationic cage through host-guest complexation, *ACS Appl. Mater. Interfaces*, 2021, **13**, 16837–16845.
47 H. H. Duan, Y. W. Li, Q. F. Li, P. P. Wang, X. R. Liu, L. Cheng, Y. Yu and L. P. Cao, Host-guest recognition and fluorescence of a tetraphenylethene-based octacationic cage, *Angew. Chem., Int. Ed.*, 2020, **59**, 10101–10110.
48 Y. Chen, G. Wu, B. Chen, H. Qu, T. Jiao, Y. Li, C. Ge, C. Zhang, L. Liang, X. Zeng, X. Cao, Q. Wang and H. Li, Self-assembly of a purely covalent cage with homochirality by imine formation in water, *Angew. Chem., Int. Ed.*, 2021, **60**, 18815–18820.
49 T. Jiao, H. Qu, L. Tong, X. Cao and H. Li, A self-assembled homochiral radical cage with paramagnetic behaviors, *Angew. Chem., Int. Ed.*, 2021, **60**, 9852–9858.
50 Y. Wang, Y. Sun, P. Shi, M. M. Sartin, X. Lin, P. Zhang, H. Fang, P. Peng, Z. Tian and X. Cao, Chaperone-like chiral cages for catalyzing enantioselective supramolecular polymerization, *Chem. Sci.*, 2019, **10**, 8076–8082.

51 H. Qu, Z. Huang, X. Dong, X. Wang, X. Tang, Z. Li, W. Gao, H. Liu, R. Huang, Z. Zhao, H. Zhang, L. Yang, Z. Tian and X. Cao, Truncated face-rotating polyhedra constructed from pentagonal pentaphenylpyrrole through graph theory, *J. Am. Chem. Soc.*, 2020, **142**, 16223–16228.
52 S. Ivanova, E. Koester, J. J. Holstein, N. Keller, G. H. Clever, T. Bein and F. Beuerle, Isoreticular crystallization of highly porous cubic covalent organic cage compounds, *Angew. Chem., Int. Ed.*, 2021, **60**, 17455–17463.
53 Y. Shi, K. Cai, H. Xiao, Z. Liu, J. Zhou, D. Shen, Y. Qiu, Q.-H. Guo, C. Stern, M. R. Wasielewski, F. Diederich, W. A. Goddard III and J. F. Stoddart, Selective extraction of C_{70} by a tetragonal prismatic porphyrin cage, *J. Am. Chem. Soc.*, 2018, **140**, 13835–13842.
54 D. Luo, Y. He, J. Tian, J. L. Sessler and X. Chi, Reversible iodine capture by nonporous adaptive crystals of a bipyridine cage, *J. Am. Chem. Soc.*, 2022, **144**, 113–117.
55 V. W. Liyana Gunawardana, T. J. Finnegan, C. E. Ward, C. E. Moore and J. D. Badjic, Dissipative formation of covalent basket cages, *Angew. Chem., Int. Ed.*, 2022, **61**, e202207418.
56 J. Koo, I. Kim, Y. Kim, D. Cho, I.-C. Hwang, R. D. Mukhopadhyay, H. Song, Y. H. Ko, A. Dhamija, H. Lee, W. Hwang, S. Kim, M.-H. Baik and K. Kim, Gigantic porphyrinic cages, *Chem*, 2020, **6**, 3374–3384.
57 S. Hong, M. R. Rohman, J. Jia, Y. Kim, D. Moon, Y. H. Ko, E. Lee and K. Kim, Porphyrin boxes: Rationally designed porous organic cages, *Angew. Chem., Int. Ed.*, 2015, **54**, 13241–13244.
58 Y. Ding, L. O. Alimi, B. Moosa, C. Maaliki, J. Jacquemin, F. Huang and N. M. Khashab, Selective adsorptive separation of cyclohexane over benzene using thienothiophene cages, *Chem. Sci.*, 2021, **12**, 5315–5318.
59 B. Moosa, L. O. Alimi, A. Shkurenko, A. Fakim, P. M. Bhatt, G. Zhang, M. Eddaoudi and N. M. Khashab, A polymorphic azobenzene cage for energy-efficient and highly selectivep-xylene separation, *Angew. Chem., Int. Ed.*, 2020, **59**, 21367–21371.
60 K. Ono, K. Johmoto, N. Yasuda, H. Uekusa, S. Fujii, M. Kiguchi and N. Iwasawa, Self-assembly of nanometer-sized boroxine cages from diboronic acids, *J. Am. Chem. Soc.*, 2015, **137**, 7015–7018.
61 B. Mondal and P. S. Mukherjee, Cage encapsulated gold nanoparticles as heterogeneous photocatalyst for facile and selective reduction of nitroarenes to azo compounds, *J. Am. Chem. Soc.*, 2018, **140**, 12592–12601.
62 S. Bera, K. Dey, T. K. Pal, A. Halder, S. Tothadi, S. Karak, M. Addicoat and R. Banerjee, Porosity switching in polymorphic porous organic cages with exceptional chemical stability, *Angew. Chem., Int. Ed.*, 2019, **58**, 4243–4247.
63 S. Bera, A. Basu, S. Tothadi, B. Garai, S. Banerjee, K. Vanka and R. Banerjee, Odd-even alternation in tautomeric porous organic cages with exceptional chemical stability, *Angew. Chem., Int. Ed.*, 2017, **56**, 2123–2126.
64 J. Sun, J. L. Bennett, T. J. Emge and R. Warmuth, Thermodynamically controlled synthesis of a chiral tetra-cavitand nanocapsule and mechanism of enantiomerization, *J. Am. Chem. Soc.*, 2011, **133**, 3268–3271.
65 M. Hua, S. Wang, Y. Gong, J. Wei, Z. Yang and J.-K. Sun, Hierarchically porous organic cages, *Angew. Chem., Int. Ed.*, 2021, **60**, 12490–12497.
66 C. Liu, Y. Jin, D. Qi, X. Ding, H. Ren, H. Wang and J. Jiang, Enantioselective assembly and recognition of heterochiral porous organic cages deduced from binary chiral components, *Chem. Sci.*, 2022, **13**, 7014–7020.
67 Q.-P. Hu, H. Zhou, T.-Y. Huang, Y.-F. Ao, D.-X. Wang and Q.-Q. Wang, Chirality gearing in an achiral cage through adaptive binding, *J. Am. Chem. Soc.*, 2022, **144**, 6180–6184.
68 H. Zhou, Y. F. Ao, D. X. Wang and Q. Q. Wang, Inherently chiral cages via hierarchical desymmetrization, *J. Am. Chem. Soc.*, 2022, **144**, 16767–16772.
69 S. Wu, Y. Ni, Y. Han, S. Xin, X. Hou, J. Zhu, Z. Li and J. Wu, Aromaticity in fully π-conjugated open-cage molecules, *J. Am. Chem. Soc.*, 2022, **144**, 23158–23167.
70 Y. Ni, T. Y. Gopalakrishna, H. Phan, T. Kim, T. S. Herng, Y. Han, T. Tao, J. Ding, D. Kim and J. Wu, 3D global aromaticity in a fully conjugated diradicaloid cage at different oxidation states, *Nat. Chem.*, 2020, **12**, 242–248.
71 P. Li, S. Xu, C. Yu, Z.-Y. Li, J. Xu, Z.-M. Li, L. Zou, X. Leng, S. Gao, Z. Liu, X. Liu and S. Zhang, De novo construction of catenanes with dissymmetric cages by space-discriminative post-assembly modification, *Angew. Chem., Int. Ed.*, 2020, **59**, 7113–7121.
72 X. Liu, G. Zhu, D. He, L. Gu, P. Shen, G. Cui, S. Wang, Z. Shi, D. Miyajima, S. Wang and S. Zhang, Guest-mediated hierarchical self-assembly of dissymmetric organic cages to form supramolecular ferroelectrics, *CCS Chem.*, 2022, **4**, 2420–2428.
73 D.-X. Cui, Y. Geng, J.-N. Kou, G.-G. Shan, C.-Y. Sun, K.-H. Zhang, X.-L. Wang and Z.-M. Su, Chiral self-sorting and guest recognition of porous aromatic cages, *Nat. Commun.*, 2022, **13**, 4011.
74 G. Montà-González, F. Sancenón, R. Martínez-Máñez and V. J. C. R. Martí-Centelles, Purely covalent molecular cages and containers for guest encapsulation, *Chem. Rev.*, 2022, **122**, 13636–13708.
75 D. Hu, J. Zhang and M. Liu, Recent advances in the applications of porous organic cages, *Chem. Commun.*, 2022, **58**, 11333–11346.
76 P. Bhandari and P. S. Mukherjee, Covalent organic cages in catalysis, *ACS Catal.*, 2023, **13**, 6126–6143.
77 W.-T. Dou, C.-Y. Yang, L.-R. Hu, B. Song, T. Jin, P.-P. Jia, X. Ji, F. Zheng, H.-B. Yang and L. Xu, Metallacages and covalent cages for biological imaging and therapeutics, *ACS Mater. Lett.*, 2023, **5**, 1061–1082.
78 S. Yu, M. Yang, Y. Liu and M. Liu, Recent advances in separation membranes based on porous organic molecular materials, *Mater. Chem. Front.*, 2023, DOI: **10.1039/d3qm00217a**.
79 D. Chakraborty and P. S. Mukherjee, Recent trends in organic cage synthesis: Push towards water-soluble organic cages, *Chem. Commun.*, 2022, **58**, 5558–5573.
80 L. Tapia, I. Alfonso and J. Sola, Molecular cages for biological applications, *Org. Biomol. Chem.*, 2021, **19**, 9527–9540.

81 K. Jie, Y. Zhou, H. P. Ryan, S. Dai and J. R. Nitschke, Engineering permanent porosity into liquids, *Adv. Mater.*, 2021, **33**, 2005745.
82 S. La Cognata, A. Miljkovic, R. Mobili, G. Bergamaschi and V. Amendola, Organic cages as building blocks for mechanically interlocked molecules: Towards molecular machines, *ChemPlusChem*, 2020, **85**, 1145–1155.
83 H.-H. Huang and T. Solomek, Photochemistry meets porous organic cages, *Chimia*, 2021, **75**, 285–290.
84 Q.-H. Ling, J.-L. Zhu, Y. Qin and L. Xu, Naphthalene diimide- and perylene diimide-based supramolecular cages, *Mater. Chem. Front.*, 2020, **4**, 3176–3189.
85 V. Ramamurthy, Photochemistry within a water-soluble organic capsule, *Acc. Chem. Res.*, 2015, **48**, 2904–2917.
86 Y. Jin, B. A. Voss, R. D. Noble and W. Zhang, A shape-persistent organic molecular cage with high selectivity for the adsorption of CO_2 over N_2, *Angew. Chem., Int. Ed.*, 2010, **49**, 6348–6351.
87 M. Mastalerz, M. W. Schneider, I. M. Oppel and O. Presly, A salicylbisimine cage compound with high surface area and selective CO_2/CH_4 adsorption, *Angew. Chem., Int. Ed.*, 2011, **50**, 1046–1051.
88 L. Chen, P. S. Reiss, S. Y. Chong, D. Holden, K. E. Jelfs, T. Hasell, M. A. Little, A. Kewley, M. E. Briggs, A. Stephenson, K. M. Thomas, J. A. Armstrong, J. Bell, J. Busto, R. Noel, J. Liu, D. M. Strachan, P. K. Thallapally and A. I. Cooper, Separation of rare gases and chiral molecules by selective binding in porous organic cages, *Nat. Mater.*, 2014, **13**, 954–960.
89 T. Hasell, M. Miklitz, A. Stephenson, M. A. Little, S. Y. Chong, R. Clowes, L. J. Chen, D. Holden, G. A. Tribello, K. E. Jelfs and A. I. Cooper, Porous organic cages for sulfur hexafluoride separation, *J. Am. Chem. Soc.*, 2016, **138**, 1653–1659.
90 M. Liu, L. Zhang, M. A. Little, V. Kapil, M. Ceriotti, S. Yang, L. Ding, D. L. Holden, R. Balderas-Xicohtencatl, D. He, R. Clowes, S. Y. Chong, G. Schutz, L. Chen, M. Hirscher and A. I. Cooper, Barely porous organic cages for hydrogen isotope separation, *Science*, 2019, **366**, 613–620.
91 Z. Wang, N. Sikdar, S.-Q. Wang, X. Li, M. Yu, X.-H. Bu, Z. Chang, X. Zou, Y. Chen, P. Cheng, K. Yu, M. J. Zaworotko and Z. Zhang, Soft porous crystal based upon organic cages that exhibit guest-induced breathing and selective gas separation, *J. Am. Chem. Soc.*, 2019, **141**, 9408–9414.
92 K. Su, W. Wang, S. Du, C. Ji and D. Yuan, Efficient ethylene purification by a robust ethane-trapping porous organic cage, *Nat. Commun.*, 2021, **12**, 3703.
93 W. Wang, K. Su, E.-S. M. El-Sayed, M. Yang and D. Yuan, Solvatomorphism influence of porous organic cage on C_2H_2/CO_2 separation, *ACS Appl. Mater. Interfaces*, 2021, **13**, 24042–24050.
94 K. Tian, S. M. Elbert, X.-Y. Hu, T. Kirschbaum, W.-S. Zhang, F. Rominger, R. R. Schroeder and M. Mastalerz, Highly selective adsorption of perfluorinated greenhouse gases by porous organic cages, *Adv. Mater.*, 2022, **34**, 2202290.
95 D. Beaudoin, F. Rominger and M. Mastalerz, Chiral self-sorting of [2+3] salicylimine cage compounds, *Angew. Chem., Int. Ed.*, 2017, **56**, 1244–1248.
96 M. W. Schneider, H.-J. Siegfried Hauswald, R. Stoll and M. Mastalerz, A shape-persistent exo-functionalized [4+6] imine cage compound with a very high specific surface area, *Chem. Commun.*, 2012, **48**, 9861–9863.
97 J. Tian, P. K. Thallapally, S. J. Dalgarno, P. B. McGrail and J. L. Atwood, Amorphous molecular organic solids for gas adsorption, *Angew. Chem., Int. Ed.*, 2009, **48**, 5492–5495.
98 K. Krishnan, J. M. Crawford, P. K. Thallapally and M. A. Carreon, Porous organic cages CC3 and CC2 as adsorbents for the separation of carbon dioxide from nitrogen and hydrogen, *Ind. Eng. Chem. Res.*, 2022, **61**, 10547–10553.
99 Y. Jin, B. A. Voss, A. Jin, H. Long, R. D. Noble and W. Zhang, Highly CO_2-selective organic molecular cages: What determines the CO_2 selectivity, *J. Am. Chem. Soc.*, 2011, **133**, 6650–6658.
100 S. Jiang, J. Bacsa, X. Wu, J. T. A. Jones, R. Dawson, A. Trewin, D. J. Adams and A. I. Cooper, Selective gas sorption in a 2 + 3 propeller cage crystal, *Chem. Commun.*, 2011, **47**, 8919–8921.
101 C. Zhang, Z. Wang, L. Tan, T.-L. Zhai, S. Wang, B. Tan, Y.-S. Zheng, X.-L. Yang and H.-B. Xu, A porous tricycloox-acalixarene cage based on tetraphenylethylene, *Angew. Chem., Int. Ed.*, 2015, **54**, 9244–9248.
102 J.-B. Xiong, J.-H. Wang, B. Li, C. Zhang, B. Tan and Y.-S. Zheng, Porous interdigitation molecular cage from tetraphenylethylene trimeric macrocycles that showed highly selective adsorption of CO_2 and tnt vapor in air, *Org. Lett.*, 2018, **20**, 321–324.
103 H. Ma, T.-L. Zhai, Z. Wang, G. Cheng, B. Tan and C. Zhang, Switching porosity of stable triptycene-based cage via solution-state assembly processes, *RSC Adv.*, 2020, **10**, 9088–9092.
104 F. Wang, E. Sikma, Z. Duan, T. Sarma, C. Lei, Z. Zhang, S. M. Humphrey and J. L. Sessler, Shape-persistent pyrrole-based covalent organic cages: Synthesis, structure and selective gas adsorption properties, *Chem. Commun.*, 2019, **55**, 6185–6188.
105 C. Liu, W. Li, Y. Liu, H. Wang, B. Yu, Z. Bao and J. Jiang, Porous organic cages for efficient gas selective separation and iodine capture, *Chem. Eng. J.*, 2022, **428**, 131129.
106 M. Yang, W. Wang, K. Su and D. Yuan, Dimeric calix 4 resorcinarene-based porous organic cages for CO_2/CH_4 separation, *Chem. Res. Chin. Univ.*, 2022, **38**, 428–432.
107 S. La Cognata, R. Mobili, C. Milanese, M. Boiocchi, M. Gaboardi, D. Armentano, J. C. Jansen, M. Monteleone, A. R. Antonangelo, M. Carta and V. Amendola, CO_2 separation by imide/imine organic cages, *Chem. – Eur. J.*, 2022, **28**, e202201631.
108 P. Wagner, F. Rominger, W.-S. Zhang, J. H. Gross, S. M. Elbert, R. R. Schroeder and M. Mastalerz, Chiral self-sorting of giant cubic 8 + 12 salicylimine cage compounds, *Angew. Chem., Int. Ed.*, 2021, **60**, 8896–8904.
109 X. Y. Hu, W. S. Zhang, F. Rominger, I. Wacker, R. R. Schroder and M. Mastalerz, Transforming a chemically labile [2 + 3] imine cage into a robust carbamate cage, *Chem. Commun.*, 2017, **53**, 8616–8619.

110 A. S. Bhat, S. M. Elbert, W.-S. Zhang, F. Rominger, M. Dieckmann, R. R. Schroeder and M. Mastalerz, Transformation of a [4 + 6] salicylbisimine cage to chemically robust amide cages, *Angew. Chem., Int. Ed.*, 2019, **58**, 8819–8823.

111 F. Qiu, X. Chen, W. Wang, K. Su and D. Yuan, Highly stable sp^2 carbon-conjugated porous organic cages, *CCS Chem.*, 2023, DOI: **10.31635/ccschem.023.202302903**.

112 M. Yang, F. Qiu, E.-S. M. El-Sayed, W. Wang, S. Du, K. Su and D. Yuan, Water-stable hydrazone-linked porous organic cages, *Chem. Sci.*, 2021, **12**, 13307–13315.

113 S. M. Elbert, N. I. Regenauer, D. Schindler, W.-S. Zhang, F. Rominger, R. R. Schroeder and M. Mastalerz, Shape-persistent tetrahedral [4 + 6] boronic ester cages with different degrees of fluoride substitution, *Chem. – Eur. J.*, 2018, **24**, 11438–11443.

114 M. Yang, X. Chen, Y. Xie, E.-S. M. El-Sayed, N. Xu, W. Wang, K. Su and D. Yuan, Post-synthetic metalation of organic cage for enhanced porosity and catalytic performance, *Sci. China-Chem.*, 2023, **66**, 1763–1770.

115 Q. Wang, T. Ke, L. Yang, Z. Zhang, X. Cui, Z. Bao, Q. Ren, Q. Yang and H. Xing, Separation of Xe from Kr with record selectivity and productivity in anion-pillared ultramicroporous materials by inverse size-sieving, *Angew. Chem., Int. Ed.*, 2020, **59**, 3423–3428.

116 R. S. Patil, D. Banerjee, C. M. Simon, J. L. Atwood and P. K. Thallapally, Noria: A highly Xe-selective nanoporous organic solid, *Chem. – Eur. J.*, 2016, **22**, 12618–12623.

117 S.-J. Lee, I.-S. Ryu, S.-G. Jeon and S.-H. Moon, Emission sources and mitigation of fluorinated non-CO_2 greenhouse gas in registered cdm projects, *Greenhouse Gases: Sci. Technol.*, 2017, **7**, 589–601.

118 A. McCulloch, Fluorocarbons in the global environment: A review of the important interactions with atmospheric chemistry and physics, *J. Fluorine Chem.*, 2003, **123**, 21–29.

119 B. K. Sovacool, S. Griffiths, J. Kim and M. Bazilian, Climate change and industrial f-gases: A critical and systematic review of developments, sociotechnical systems and policy options for reducing synthetic greenhouse gas emissions, *Renewable Sustainable Energy Rev.*, 2021, **141**, 110759.

120 I. Krkljus, T. Steriotis, G. Charalambopoulou, A. Gotzias and M. Hirscher, H_2/D_2 adsorption and desorption studies on carbon molecular sieves with different pore structures, *Carbon*, 2013, **57**, 239–247.

121 X. B. Zhao, S. Villar-Rodil, A. J. Fletcher and K. M. Thomas, Kinetic isotope effect for H_2 and D_2 quantum molecular sieving in adsorption/desorption on porous carbon materials, *J. Phys. Chem. B*, 2006, **110**, 9947–9955.

122 D. Cao, H. Huang, Y. Lan, X. Chen, Q. Yang, D. Liu, Y. Gong, C. Xiao, C. Zhong and S. Peng, Ultrahigh effective H_2/D_2 separation in an ultramicroporous metal–organic framework material through quantum sieving, *J. Mater. Chem. A*, 2018, **6**, 19954–19959.

123 L. Zhang, T. Wulf, F. Baum, W. Schmidt, T. Heine and M. Hirscher, Chemical affinity of Ag-exchanged zeolites for efficient hydrogen isotope separation, *Inorg. Chem.*, 2022, **61**, 9413–9420.

124 J. Y. Kim, J. Park, J. Ha, M. Jung, D. Wallacher, A. Franz, R. Balderas-Xicohtencatl, M. Hirscher, S. G. Kang, J. T. Park, I. H. Oh, H. R. Moon and H. Oh, Specific isotope-responsive breathing transition in flexible metal-organic frameworks, *J. Am. Chem. Soc.*, 2020, **142**, 13278–13282.

125 J. Y. Kim, H. Oh and H. R. Moon, Hydrogen isotope separation in confined nanospaces: Carbons, zeolites, metal-organic frameworks, and covalent organic frameworks, *Adv. Mater.*, 2019, **31**, e1805293.

126 X. Yan, Y. Song, D. Wang, T. Xia, X. Tan, J. Ba, T. Tang, W. Luo, G. Sang and R. Xiong, Direct observation of highly effective hydrogen isotope separation at active metal sites by in situ drift spectroscopy, *Chem. Commun.*, 2023, **59**, 3922–3925.

127 Y. Si, X. He, J. Jiang, Z. Duan, W. Wang and D. Yuan, Highly effective H_2/D_2 separation in a stable Cu-based metal-organic framework, *Nano Res.*, 2019, **14**, 518–525.

128 D. J. Vogel, T. M. Nenoff and J. M. Rimsza, Design elements for enhanced hydrogen isotope separations in barely porous organic cages, *ACS Omega*, 2022, **7**, 7963–7972.

129 H. Wang and J. Li, Microporous metal-organic frameworks for adsorptive separation of C5-C6 alkane isomers, *Acc. Chem. Res.*, 2019, **52**, 1968–1978.

130 J.-W. Cao, S. Mukherjee, T. Pham, Y. Wang, T. Wang, T. Zhang, X. Jiang, H.-J. Tang, K. A. Forrest, B. Space, M. J. Zaworotko and K.-J. Chen, One-step ethylene production from a four-component gas mixture by a single physisorbent, *Nat. Commun.*, 2021, **12**, 6507.

131 P.-Q. Liao, N.-Y. Huang, W.-X. Zhang, J.-P. Zhang and X.-M. Chen, Controlling guest conformation for efficient purification of butadiene, *Science*, 2017, **356**, 1193–1196.

132 H. Zeng, M. Xie, T. Wang, R.-J. Wei, X.-J. Xie, Y. Zhao, W. Lu and D. Li, Orthogonal-array dynamic molecular sieving of propylene/propane mixtures, *Nature*, 2021, **595**, 542–548.

133 R.-B. Lin and B. Chen, A dynamic mof for efficient purification of propylene, *Sci. China-Chem.*, 2021, **64**, 2053–2054.

134 S. Horike, S. Shimomura and S. Kitagawa, Soft porous crystals, *Nat. Chem.*, 2009, **1**, 695–704.

135 K. Qu, J. Xu, L. Dai, Y. Wang, H. Cao, D. Zhang, Y. Wu, W. Xu, K. Huang, C. Lian, X. Guo, W. Jin and Z. Xu, Electrostatic-induced crystal-rearrangement of porous organic cage membrane for CO_2 capture, *Angew. Chem., Int. Ed.*, 2022, **61**, e202205481.

136 T. T. Xu, B. Wu, L. X. Hou, Y. R. Zhu, F. M. Sheng, Z. Zhao, Y. Dong, J. D. Liu, B. J. Ye, X. Y. Li, L. Ge, H. T. Wang and T. W. Xu, Highly ion-permselective porous organic cage membranes with hierarchical channels, *J. Am. Chem. Soc.*, 2022, **144**, 10220–10229.

137 Y. D. Yuan, J. Dong, J. Liu, D. Zhao, H. Wu, W. Zhou, H. X. Gan, Y. W. Tong, J. Jiang and D. Zhao, Porous organic cages as synthetic water channels, *Nat. Commun.*, 2020, **11**, 4927.

138 A. He, Z. Jiang, Y. Wu, H. Hussain, J. Rawle, M. E. Briggs, M. A. Little, A. G. Livingston and A. I. Cooper, A smart and responsive crystalline porous organic cage membrane with switchable pore apertures for graded molecular sieving, *Nat. Mater.*, 2022, **21**, 463–470.